NASA/TP-1998-208464

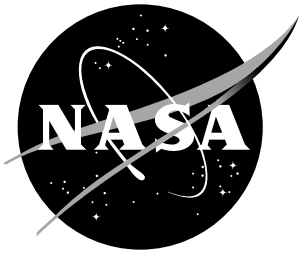

A Method for Integrating Thrust-Vectoring and Actuated Forebody Strakes With Conventional Aerodynamic Controls on a High-Performance Fighter Airplane

Frederick J. Lallman, John B. Davidson, and Patrick C. Murphy
Langley Research Center, Hampton, Virginia

September 1998

The NASA STI Program Office ... in Profile

Since its founding, NASA has been dedicated to the advancement of aeronautics and space science. The NASA Scientific and Technical Information (STI) Program Office plays a key part in helping NASA maintain this important role.

The NASA STI Program Office is operated by Langley Research Center, the lead center for NASA's scientific and technical information. The NASA STI Program Office provides access to the NASA STI Database, the largest collection of aeronautical and space science STI in the world. The Program Office is also NASA's institutional mechanism for disseminating the results of its research and development activities. These results are published by NASA in the NASA STI Report Series, which includes the following report types:

- TECHNICAL PUBLICATION. Reports of completed research or a major significant phase of research that present the results of NASA programs and include extensive data or theoretical analysis. Includes compilations of significant scientific and technical data and information deemed to be of continuing reference value. NASA counter-part of peer reviewed formal professional papers, but having less stringent limitations on manuscript length and extent of graphic presentations.

- TECHNICAL MEMORANDUM. Scientific and technical findings that are preliminary or of specialized interest, e.g., quick release reports, working papers, and bibliographies that contain minimal annotation. Does not contain extensive analysis.

- CONTRACTOR REPORT. Scientific and technical findings by NASA-sponsored contractors and grantees.

- CONFERENCE PUBLICATION. Collected papers from scientific and technical conferences, symposia, seminars, or other meetings sponsored or co-sponsored by NASA.

- SPECIAL PUBLICATION. Scientific, technical, or historical information from NASA programs, projects, and missions, often concerned with subjects having substantial public interest.

- TECHNICAL TRANSLATION. English-language translations of foreign scientific and technical material pertinent to NASA's mission.

Specialized services that help round out the STI Program Office's diverse offerings include creating custom thesauri, building customized databases, organizing and publishing research results ... even providing videos.

For more information about the NASA STI Program Office, see the following:

- Access the NASA STI Program Home Page at ***http://www.sti.nasa.gov***

- E-mail your question via the Internet to help@sti.nasa.gov

- Fax your question to the NASA Access Help Desk at (301) 621-0134

- Phone the NASA Access Help Desk at (301) 621-0390

- Write to:
  NASA Access Help Desk
  NASA Center for AeroSpace Information
  7121 Standard Drive
  Hanover, MD 21076-1320

NASA/TP-1998-208464

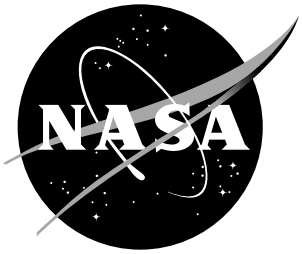

A Method for Integrating Thrust-Vectoring and Actuated Forebody Strakes With Conventional Aerodynamic Controls on a High-Performance Fighter Airplane

Frederick J. Lallman, John B. Davidson, and Patrick C. Murphy
Langley Research Center, Hampton, Virginia

National Aeronautics and
Space Administration

Langley Research Center
Hampton, Virginia 23681-2199

September 1998

The use of trademarks or names of manufacturers in the report is for accurate reporting and does not constitute an official endorsement, either expressed or implied, of such products or manufacturers by the National Aeronautics and Space Administration.

Available from the following:

NASA Center for AeroSpace Information (CASI)
7121 Standard Drive
Hanover, MD 21076-1320
(301) 621-0390

National Technical Information Service (NTIS)
5285 Port Royal Road
Springfield, VA 22161-2171
(703) 487-4650

Contents

Abstract

A method, called pseudo controls, of integrating several airplane controls to achieve cooperative operation is presented. The method eliminates conflicting control motions, minimizes the number of feedback control gains, and reduces the complication of feedback gain schedules. The method is applied to the lateral/directional controls of a modified high-performance airplane. The airplane has a conventional set of aerodynamic controls, an experimental set of thrust-vectoring controls, and an experimental set of actuated forebody strakes. The experimental controls give the airplane additional control power for enhanced stability and maneuvering capabilities while flying over an expanded envelope, especially at high angles of attack.

The flight controls are scheduled to generate independent body-axis control moments. These control moments are coordinated to produce stability-axis angular accelerations. Inertial coupling moments are compensated. Thrust-vectoring controls are engaged according to their effectiveness relative to that of the aerodynamic controls. Vane-relief logic removes steady and slowly varying commands from the thrust-vectoring controls to alleviate heating of the thrust turning devices. The actuated forebody strakes are engaged at high angles of attack.

This report presents the forward-loop elements of a flight control system that positions the flight controls according to desired stability-axis accelerations. This report does not include the generation of the required angular acceleration commands by means of pilot controls or the feedback of sensed airplane motions.

Summary

The pseudo controls method for integrating lateral/directional aerodynamic and thrust-vectoring controls on fighter-type jet airplanes is presented. The NASA High-Alpha Research Vehicle (HARV) discussed in this report is a modern high-performance twin-engine jet fighter that is modified to carry an experimental thrust-vectoring apparatus and an experimental set of actuated forebody strakes. The experimental controls augment the conventional aerodynamic controls (ailerons, twin rudders, and a horizontal stabilator capable of differential deflections) to extend the flight envelope to high angles of attack and slow airspeeds.

The purpose of the pseudo controls method is to integrate the conventional aerodynamic controls with experimental thrust-vectoring and actuated forebody strake controls. The pseudo controls method organizes the aerodynamic and thrust-vectoring control activity to cause moments about the airplane axes that satisfy the demands of stability augmentation feedback loops, pilot commands, and inertial decoupling. The pseudo controls method converts stability-axis roll and yaw angular acceleration commands into coordinated control deflections. This reduces the number of commanded items from the number of controls available to commanded roll and yaw accelerations and simplifies the task of the designer of the feedback part of the control system. The acceleration commands are generated from pilot control inputs and stabilizing feedback sensor signals. This may be accomplished by any accepted control law design method and is not addressed in this report. The acceleration commands are distributed

to the control effectors in proportions that are scheduled according to flight conditions. Distribution gains are determined for the conventional controls to separate body-axis rolling and yawing control moments. The thrust-vectoring and actuated forebody strake controls are specifically designed to generate moments about the body axes. The actuated forebody strakes engage when the angle of attack is at least 20 degrees. Thrust-vectoring controls engage when their control moment producing capabilities are comparable to that of the aerodynamic controls. The conventional aerodynamic control deflections are adjusted to compensate for the increased control power made available by the thrust-vectoring and actuated forebody strake controls. To minimize heating of the thrust-turning vanes, a vane relief algorithm was developed to replace steady thrust-vectoring commands by increased deflections of the aerodynamic controls.

The development of the pseudo controls method and its application to the HARV airplane as described in this report were performed under the NASA High-Alpha Technology Program (HATP).

Introduction

One key element in the evolution of fighter airplane designs into more effective configurations is the ability to fly at increasing angles of attack. New types of control devices allow flight operations that are beyond the reach of conventional airplanes. Vectored thrust and forebody controls can provide control power to maintain stable and effective flight in the post-stall regime. Control system designs using these new, effective devices can provide safe maneuverability at post-stall angles of attack with inherent departure and spin resistance. In addition, the availability of control power during post-stall flight creates new opportunities for gaining tactical advantage over an adversary.

A number of airplanes have achieved controlled flight in the post-stall regime. The Grumman Aircraft Corporation X-29 Forward Swept Wing Technology Demonstrator airplane achieved controlled flight at post-stall angles of attack because of its unique wing design and close-coupled canards (reference 1). The Rockwell International Corporation's North American Aircraft & Deutsche Aerospace (formerly Messerschmitt-Bolkow-Blohm) X-31 Enhanced Fighter Maneuverability Demonstrator, the Lockheed Fort Worth Company F-16 Multi-Axis Thrust Vectoring (MATV), and the Lockheed Advanced Development Company, The Boeing Company & General Dynamics YF-22 Advanced Tactical Fighter prototype (reference 2) have reached angles of attack of 60° or more because of their use of thrust-vectoring controls. Another airplane that has flown these high angles of attack is the National Aeronautics and Space Administration (NASA) F-18 High Angle-of-Attack Research Vehicle (HARV). The HARV airplane (figure 1) flew in support of the NASA High-Angle-of-Attack Technology Program (HATP). HATP was a technology development and validation program for fighter airplanes possessing high angle-of-attack maneuverability and controllability (reference 3). The program used analysis, ground-based testing, simulation, and flight tests to advance technology in aerodynamics, advanced controls, and maneuver management. The HARV airplane achieved controlled flight up to 60 degrees angle of attack and was the first airplane to use active forebody controls (actuated strakes) to enhance rolling maneuvers. The present report describes a method of integrating new post-stall control effectors with conventional aerodynamic controls that was part of an experimental high angle-of-attack flight control system developed for HARV.

The HATP program used the HARV as a flight test vehicle to validate high angle-of-attack control designs and to gather flight test data. The HARV airplane was a full-scale developmental twin-engine, single-place, fighter/attack (F/A) airplane. It was built for the US Navy by the McDonnell Douglas Corp.

Figure 1. The High Angle-of-Attack Research Vehicle (HARV).[1]

(St. Louis, MO) and the Northrop Corp. (Newbury Park, CA) and was previously used for high angle of attack and spin testing. The HARV was powered by two General Electric (Lynn, MA) F404-GE-400 afterburning turbofan engines.

Several modifications were made to the airplane to prepare it for flight tests (references 4 and 5). A research flight control system (RFCS) using Pace 1750A computers (Performance Semiconductor Corp., Sunnyvale, CA) was added to the airplane avionics. Research control laws and flight test software were programmed in the RFCS computers. An emergency spin recovery parachute assembly was mounted to the upper aft portion of the airplane between the engines. High angle-of-attack in-flight flow visualization and pressure measurement equipment was installed. Flight-test instrumentation and real-time air-to-ground data links were installed. Various indicators, switches, etc., were provided in the cockpit to allow the pilot to monitor and control the special flight test equipment.

Turning vanes were added to the HARV to provide thrust-vectoring capability (figure 2). In order to accommodate the vane installation, the engines were modified by removing the divergent flap portion of the nozzle. The convergent nozzle hardware was modified to maintain structural integrity and the engine controller was modified to increase the engine stall margin. The inside trailing edges of the stabilators were modified slightly to provide clearance for the thrust-vectoring hardware.

Three vanes were positioned about the periphery of each engine nozzle. The vanes were made of Inconel 625® steel and each was moved by a modified aileron electrohydraulic actuator. The larger top vanes generate nose-down pitching moments, while the smaller lower (inboard and outboard) vanes moved collectively to generate nose-up pitching moments. Other combinations of vane positions were designed to cause the generation of yaw and rolling moments.

In order to initially evaluate the vectoring capability and isolated nozzle performance of the thrust-vectoring system, a static (wind-off) test was conducted on a 14.25 percent scaled model. Vane sizes and actuation geometries were tested over a range of deflections and nozzle pressure ratios with military-power and afterburning-power nozzles. The test examined the effects of vane deflections on thrust vectoring and resultant thrust losses. The test results favored the simple rotating vane actuation system that was implemented on the HARV airplane over a more complicated translating-rotating vane concept (reference 6).

---

[1]Photographs supplied by NASA Dryden Flight Research Center, Edwards, CA.

®Inconel 625 is a registered trademark of Huntington Alloy Products Division, International Nickel Co., Huntington, WV.

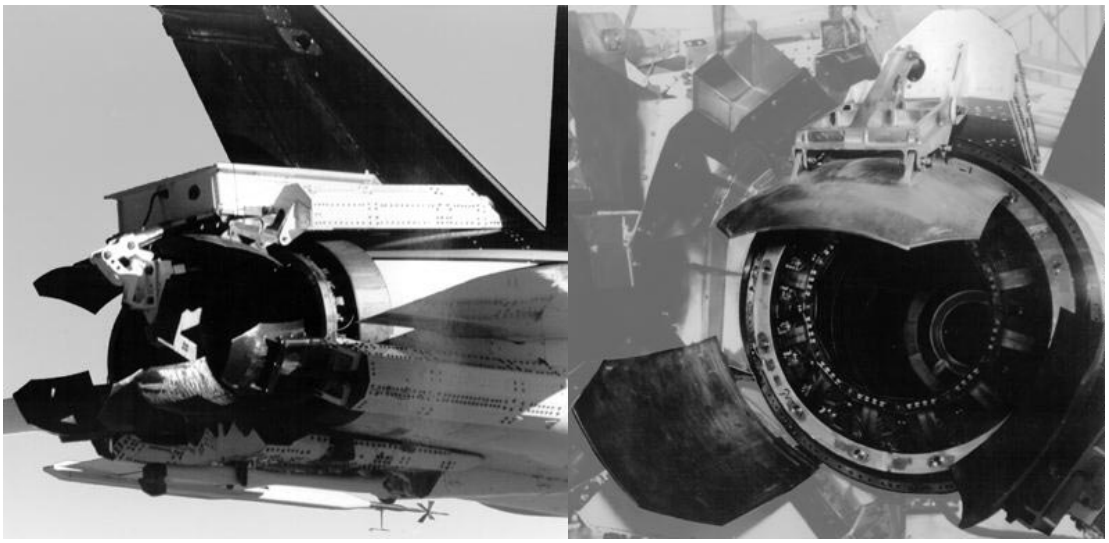

Figure 2. HARV Thrust-Vectoring System.

A wingtip-supported, partially metric, 0.10-scale (cold) jet-effects model of an F-18 prototype aircraft was modified with hardware to simulate the thrust-vectoring control system of the HARV. Afterbody aerodynamic and thrust-vectoring forces and moments were measured at free-stream Mach numbers ranging from 0.30 to 0.70, at angles of attack from 0° to 70°, and at nozzle pressure ratios from 1.0 to 5.0 with afterburning and military power nozzles (reference 7). These data were used to design a Mixer/Predictor program that could position the vanes to get commanded pitch, yaw, and roll moments (reference 8). The HARV experiments used pitch and yaw thrust-vectoring moments to maintain stable flight at high angles of attack. The roll thrust-vectoring capability was not used in the flight test program because the roll moments produced were limited by priority logic in the Mixer/Predictor program. Figure 3 shows the thrust-vectoring system deflecting engine thrust during a propulsion system test.

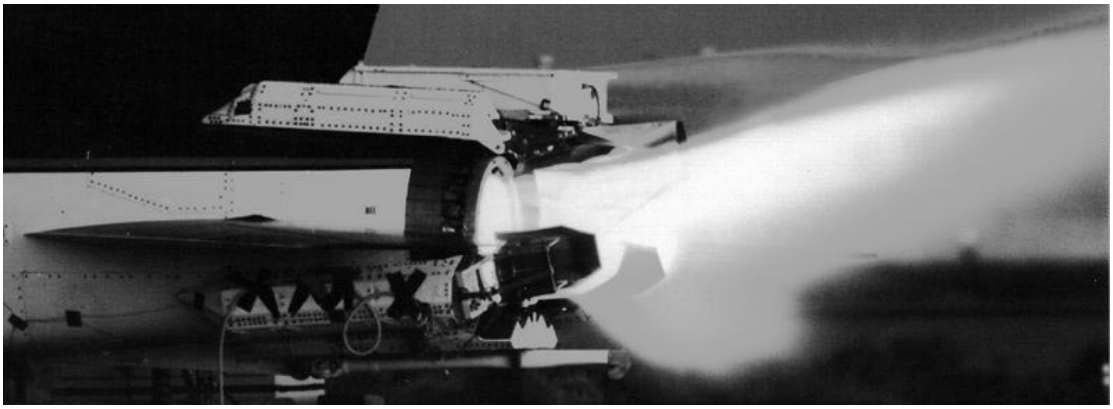

Figure 3. HARV Thrust Vectoring Test.

The HARV airplane initially flew with thrust-vectoring controls during 1991. A flight test program established the utility of thrust-vectoring controls and demonstrated controlled, maneuvering flight at post-stall angles of attack. The flight control law used at that time was developed jointly by NASA and McDonnell Aircraft Company. A second thrust-vectoring control law, known as the NASA-1A control

law, was developed at NASA Langley Research Center. The NASA-1A control law was flown on the HARV during 1994.

The radome of the HARV was replaced with a specially built radome that includes a pair of longitudinally hinged, actuated forebody strakes (reference 9). Deployment of the strakes (figure 4) changes the flow separation and vortices shed from the airplane forebody when flying at high angles of attack. Wind-tunnel tests predicted that the yawing moments resulting from differential strake deflections would provide a powerful means of controlling the HARV at high angles of attack (references 9 and 10).

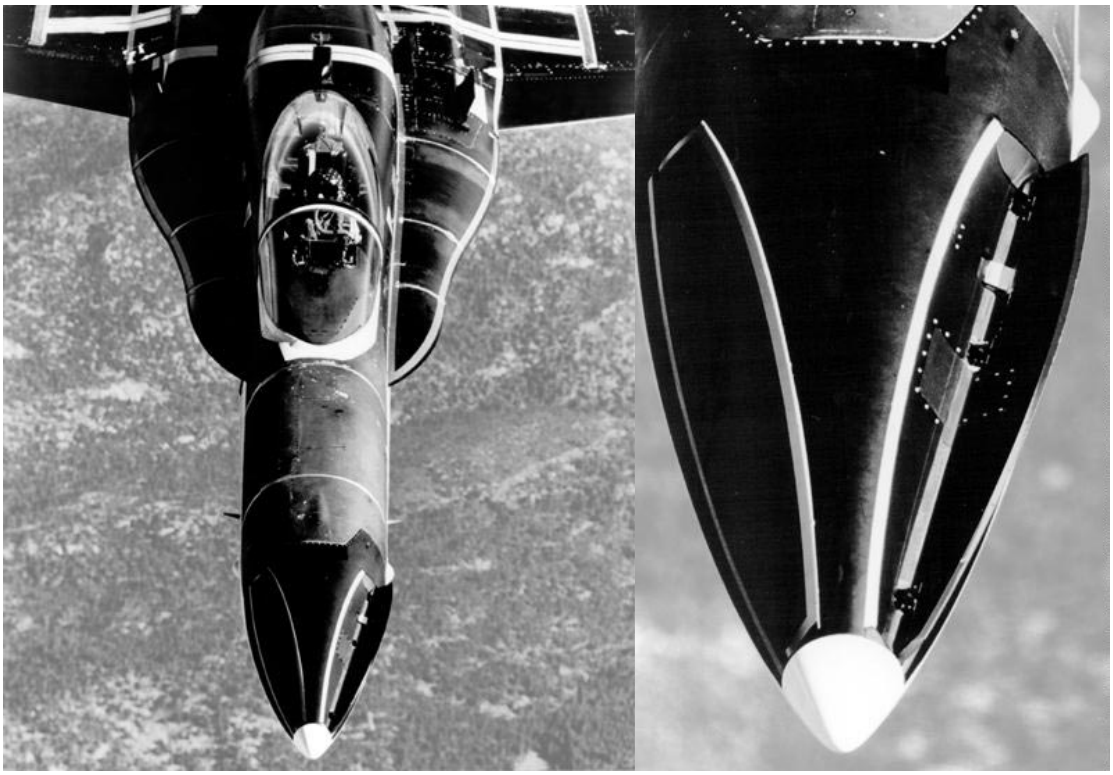

Figure 4. HARV Airplane with Left Actuated Forebody Strake Deployed.

The radome and actuated forebody strake structures consisted of aluminum skin panels riveted to aluminum stringers and bulkheads. The strakes were moved by F-18 aileron actuators modified for longer strokes and faster rates. When closed (0° deflection), the strakes conformed to the normal shape of the F-18 radome. The strakes could be independently commanded up to 90° deflections within 1/2 second.

Flight control laws that used the actuated forebody strakes and the thrust-vectoring system were developed at NASA Langley Research Center and are known as the ANSER (Actuated Nose Strakes for Enhanced Rolling) Control Laws. A detailed specification of the ANSER control law is given in reference 11. The control laws were tailored to satisfy a number of performance and handling quality design guidelines (reference 12). The ANSER control law used a “mixer-predictor” to position the thrust-vectoring vanes in response to multiaxis thrust-vector angle commands (reference 8). A longitudinal controller consisted of a variable-gain output-feedback controller, a feed-forward command generator, and a command generator tracker (reference 13). The longitudinal controller used horizontal tail

deflections and pitch-axis thrust vectoring to achieve rapid (agile) pitching motions to commanded angles of attack. The leading-edge and trailing-edge flaps follow the schedules of the production F/A-18 airplane. The lateral/directional controller used stability-axis roll and yaw angular accelerations to control stability-axis roll rate and sideslip angle. Feedback control gain schedules were calculated using direct eigenspace assignment with tradeoffs among control power, robustness, agility, and flying qualities metrics (reference 14). The control laws were programmed in the FORTRAN programming language for ground-based testing. A simulation program of a baseline F/A-18 airplane (reference 15) was modified to represent the HARV airplane including the TVCS and ANSER controls (reference 16). Testing of these programs was performed by an ACSL (Advanced Continuous Simulation Language, reference 17) batch-mode simulation. Piloted evaluation of the HARV airplane and the ANSER control laws was conducted in the Differential Maneuvering Simulator (DMS) at NASA Langley Research Center (reference 18). The DMS is a fixed-based simulator having wide-angle visual displays and is capable of simulating two airplanes as they maneuver relative to each other. The evaluations used a series of piloting tasks designed to test the longitudinal and the lateral/directional control systems throughout the HARV flight envelope (reference 12). The ANSER control laws were installed in the RFCS computers onboard the HARV airplane and hardware-in-the-loop simulations at NASA Dryden Flight Research Facility. The flight tests were designed to provide aerodynamic measurements, flow field visualizations, airplane controllability, and agility ratings. These flight tests were conducted from 1995 to 1996 at NASA Dryden Flight Research Facility.

One challenge of the ANSER control system was to determine how to best schedule the many control effectors, especially at high angles of attack. The organization of these controls to provide independent channels of control of lateral and directional motions throughout the flight test envelope was accomplished by using the pseudo controls method. An early version of the pseudo controls method is described in references 19 and 20 for a jet fighter configuration having roll and yaw thrust-vectoring capabilities in addition to ailerons, rudder, and differential horizontal tail available for control. The controls were coordinated to form one control channel that affected the Dutch roll mode and another channel that affected the roll and spiral modes of the airplane (reference 19). This method was applied over a range of trimmed, level flight conditions to produce schedules that distributed the individual channel commands among the four control effectors. Feedback loops were added and batch simulation results demonstrated promising results. Lateral control stick deflections caused stability-axis roll rates with small Dutch roll excitation and rudder pedal deflections caused steady sideslips with small steady-state roll rates (reference 20).

The pseudo controls method was applied to the mathematical model of the HARV airplane as a way of coordinating all its lateral/directional controls and reducing the number of feedback control channels. For the HARV airplane, an envelope was defined over a wide range of angle of attack, Mach number, and engine thrust settings without reference to trimmed flight. Unfortunately, the calculated distributions were very sensitive at some conditions and it was felt that the scheduling of the results of the early pseudo controls method would be impractical for the HARV airplane. The pseudo controls method was modified for use on the HARV airplane. The lateral and directional control channels were configured to produce stability-axis accelerations instead of affecting the dynamic modes of motion as was previously attempted. The remainder of this report provides a detailed description of the modified pseudo controls method as it was implemented on the HARV airplane.

Symbols and Nomenclature

Numerical values, where given, are nominal values for the HARV airplane.

Symbol	Value	Unit	Description
ANSER	–	–	Actuated Nose Strakes for Enhanced Rolling
AOA	–	degree	angle of attack
a_y	–	ft/sec^2	lateral acceleration at the sensor location
a_{cg}	–	ft/sec^2	lateral acceleration at the center of gravity
$a_{y,corr}$	–	ft/sec^2	lateral accelerometer correction
$a_{y,TV}$	–	ft/sec^2 per ft-lb	interference of thrust vectoring on lateral accelerometer
$a_{y,FS}$	–	ft/sec^2 per ft-lb	interference of actuated forebody strakes on lateral accelerometer
b	37.42	ft	wing span
$\overrightarrow{c_{roll}}$	–	ft-lb	3-vector of roll moments
$\overrightarrow{c_{yaw}}$	–	ft-lb	3-vector of yaw moments
$\vec{d}$	–	–	solution of optimization problem
c.g.	–	–	center of gravity
$C_{l\delta a}$	–	deg^{-1}	aileron roll control derivative
$C_{l\delta d}$	–	deg^{-1}	differential tail roll control derivative
$C_{l\delta r}$	–	deg^{-1}	rudder roll control derivative
$C_{n\delta a}$	–	deg^{-1}	aileron yaw control derivative
$C_{n\delta d}$	–	deg^{-1}	differential tail yaw control derivative
$C_{n\delta r}$	–	deg^{-1}	rudder yaw control derivative
C_{roll}	–	–	aerodynamic roll moment coefficient available from conventional controls
C_{yaw}	–	–	aerodynamic yaw moment coefficient available from conventional controls
CRAFT			Control power, Robustness, Agility, and Flying qualities Tradeoffs
$\overrightarrow{d_{roll}}$	–	–	roll distribution 3-vector
$\overrightarrow{d_{yaw}}$	–	–	yaw distribution 3-vector
F_{aero}	–	pound	lateral aerodynamic force including conventional controls
F_{FS}	–	pound	lateral force of actuated forebody strakes
F_{TV}	–	pound	lateral thrust-vectoring force
HARV	–	–	High-Angle-of-Attack Research Vehicle

Symbol	Value	Unit	Description
HATP	–	–	High-Alpha Technology Program
I_{XX}	22 632	slug-ft^2	moment of inertia (roll axis)
I_{XZ}	–2131.8	slug-ft^2	product of inertia
I_{YY}	174 246.3	slug-ft^2	moment of inertia (pitch axis)
I_{ZZ}	189 336.4	slug-ft^2	moment of inertia (yaw axis)
J	–	(ft-lb)^2	performance index for optimization problem
KEAS	–	knots	knots equivalent airspeed
L	–	ft-lb	roll control moment
L_{aero}	–	ft-lb	aerodynamic roll moment available from conventional controls
L_{avail}	–	ft-lb	available roll control moment for $v_{roll} = 1$
L_{cmd}	–	ft-lb	commanded roll control moment
L_{TV}	–	ft-lb	available roll thrust-vector control moment
l_a	12.46	ft	distance from c.g. to lateral accelerometer
l_{FS}	–	ft	effective forebody strake moment arm
l_{TV}	20.3	ft	distance from c.g. to the TV nozzles
l_y	1.53	ft	lateral distance from centerline to nozzles
l_z	0.45	ft	distance TV nozzles below c.g.
M	–	ft-lb	total control moment §
M_A	–	ft-lb	available aerodynamic control moment §
M_C	–	ft-lb	commanded control moment §
M_{TV}	–	ft-lb	available thrust-vectoring control moment §
m	1111.6	slug	mass of airplane
N	–	ft-lb	yaw control moment
N_{aero}	–	ft-lb	aerodynamic yaw moment available from conventional controls
N_{avail}	–	ft-lb	available yaw control moment for $v_{yaw} = 1$
N_{cmd}	–	ft-lb	commanded yaw control moment
N_{FS}	–	ft-lb	commanded actuated forebody strake yaw control moment
N_{TV}	–	ft-lb	available yaw thrust-vector control moment
p	–	rad/sec	body-axis roll rate
$\dot{p}_{cmd}$	–	rad/sec^2	commanded body-axis roll acceleration
$\dot{p}_{max}$	–	rad/sec^2	body-axis roll acceleration capability
$\dot{p}_s$	–	rad/sec^2	stability-axis roll acceleration

§variable may refer to either roll or yaw axis depending on application.

Symbol	Value	Unit	Description
$\dot{p}_{s,max}$	–	rad/sec^2	maximum stability-axis roll acceleration
q	–	rad/sec	body-axis pitch rate
$\bar{q}$	–	lb/ft2	dynamic pressure
r	–	rad/sec	body-axis yaw rate
$\dot{r}$	–	rad/sec^2	body-axis yaw acceleration
$\dot{r}_{cmd}$	–	rad/sec^2	commanded body-axis yaw acceleration
$\dot{r}_{max}$	–	rad/sec^2	body-axis yaw acceleration capability
$\dot{r}_s$	–	rad/sec^2	stability-axis yaw acceleration
S	400	ft^2	reference wing area
S_{TV}	0 to 1	–	thrust-vectoring engagement variable
S_{TVr}	0 to 1	–	roll TV engagement variable
S_{TVy}	0 to 1	–	yaw TV engagement variable
T	–	lb	total engine thrust
T_c	–	sec	vane relief filter time constant §
TED	–	–	trailing edge down
TEU	–	–	trailing edge up
TV	–	–	Thrust Vector
$\vec{u}$	–	–	3-vector of normalized control deflections
V	–	ft/sec	velocity
v_A	–1 to +1	–	aerodynamic pseudo control variable §
$v_{A,nom}$	–1 to +1	–	nominal aerodynamic pseudo control variable §
v_C	–1 to +1	–	command pseudo control variable §
v_{dir}	–	rad/sec^2	directional pseudo control variable
v_{lat}	–	rad/sec^2	lateral pseudo control variable
v_{roll}	–1 to +1	–	roll pseudo control variable
v_{TV}	–1 to +1	–	thrust-vectoring pseudo control variable §
$v_{TV,nom}$	–1 to +1	–	nominal thrust-vectoring pseudo control variable §
v_{yaw}	–1 to +1	–	yaw pseudo control variable
W	–	(ft-lb)^2	(3×3) matrix (products of moment coefficients)
α	–	degree	angle of attack
$\Delta C_{l\delta a}$	–	–	roll moment coefficient for maximum aileron deflection
$\Delta C_{l\delta d}$	–	–	roll moment coefficient for maximum differential stabilator deflection

§variable may refer to either roll or yaw axis depending on application.

Symbol	Value	Unit	Description
$\Delta C_{l\delta r}$	–	–	roll moment coefficient for maximum rudder deflection
$\Delta C_{n\delta a}$	–	–	yaw moment coefficient for maximum aileron deflection
$\Delta C_{n\delta d}$	–	–	yaw moment coefficient for maximum differential stabilator deflection
$\Delta C_{n\delta r}$	–	–	yaw moment coefficient for maximum rudder deflection
$\Delta C_{n,FS}$	–	–	yaw moment coefficient for maximum actuated forebody strake deflection
Δv_A	±1	–	aerodynamic vane relief increment §
$\Delta v_{A,filt}$	±1	–	filtered aerodynamic vane relief increment §
δ_a	–	degree	aileron deflection angle
δ_{am}	25.0	degree	maximum aileron deflection angle
δ_d	–	degree	differential tail deflection angle
δ_{dm}	17.25*	degree	maximum differential tail deflection angle
δ_{FS}	±90.0	degree	maximum differential actuated forebody strake deflection
δ_r	–	degree	rudder deflection angle
δ_{rm}	30.0	degree	maximum rudder deflection angle
δ_{TVr}	–	degree	rolling thrust-vector angle
δ_{TVrm}	15.0	degree	maximum rolling thrust-vector angle
δ_{TVy}	–	degree	yawing thrust-vector angle
δ_{TVym}	10.0	degree	maximum yawing thrust-vector angle

§variable may refer to either roll or yaw axis depending on application.
*each horizontal tail surface deflects from –24.0 to +10.5 degrees.

Pseudo Controls Overview

This section presents a brief overview of the integrated lateral/directional controls system designed for the HARV airplane. The system as shown in figure 5 is partitioned into a feedback control portion and a pseudo control portion. The feedback controls, depicted on the left side of the figure, combine signals from the pilot controls and the airplane sensors to calculate the airplane accelerations required for stability in flight and response to piloting commands. The feedback gains are calculated using the CRAFT methodology reported in reference 14. This process uses Direct Eigenspace Assignment to make the airplane's stability characteristics have level 1 (satisfactory) flying qualities where possible. Lateral control stick gains are scheduled to achieve the roll rates specified by the design guidelines reported in reference 12. Rudder pedal gains are scheduled to achieve 10 degrees of sideslip angle. Lateral control stick and rudder pedal signals are cross-fed to minimize the angle of sideslip during rolling maneuvers.

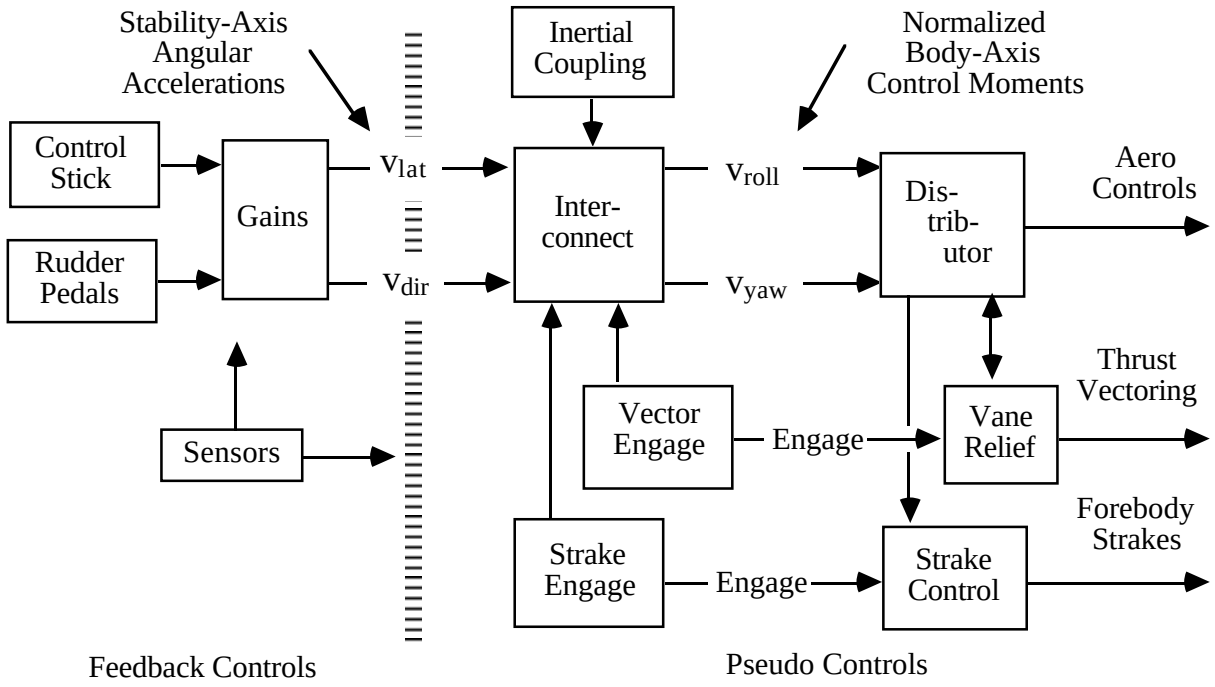

Figure 5. Lateral/Directional Control System Overview.

The pseudo controls portion, the subject of this report, positions the conventional aerodynamic control surfaces (aileron, rudders, and differential stabilators), the thrust-vectoring mechanisms, and the actuated forebody strakes in response to the acceleration commands generated from pilot command and sensor feedbacks. The stability-axis roll acceleration is v_{lat}, rad/sec^2, and the stability-axis yaw acceleration is v_{dir}, rad/sec^2. The amounts of body-axis roll and yaw control moments needed to produce these accelerations are calculated, including moments needed to counter inertial coupling effects. Calculations are made of the available control moments from the conventional controls, the thrust-vector controls, and the actuated forebody strakes. The ratios of the required moments to the available moments become the pseudo control variables v_{roll} and v_{yaw}. These are used to drive the aerodynamic controls according to schedules that decouple roll and yaw moments. Some of the control moments may be produced by the thrust-vectoring controls and the actuated forebody strakes. A vane relief function is used to transfer slow, steady deflections from the thrust-vectoring controls to the aerodynamic controls. A more detailed development of the pseudo controls portion of the control law is given in the following sections.

Controls Interconnect

This section describes the transformation of lateral/directional angular acceleration commands into roll and yaw pseudo control variables. The lateral acceleration command, v_{lat}, is an instantaneous angular acceleration command about the stability x-axis that causes rolling motions, generally about the velocity vector. The directional acceleration command, v_{dir} is an instantaneous angular acceleration about the stability z-axis that causes yawing motions perpendicular to the velocity vector to produce sideslip. These commands are generated from combinations of pilot commands and sensor feedbacks. The controls interconnect transforms the acceleration commands into body-axis pseudo control variables that are then distributed to the individual control effectors as described in a following section. The interconnect includes compensation for inertial coupling effects.

Axis Transformation

The commands from the feedback controls to pseudo controls are the lateral pseudo control variable, v_{lat}, and the directional pseudo control variable, v_{dir}. The lateral pseudo control variable commands an instantaneous angular acceleration about the velocity vector that is a combined rolling and yawing acceleration about the airplane body axes as is shown in figure 6a. The directional pseudo control variable commands an instantaneous acceleration about an axis that is perpendicular to the velocity vector as is shown in figure 6b. The lateral and directional pseudo control variables are combined in the following axis-transformation formulas (1) to produce the body-axis acceleration commands.

$$\begin{bmatrix} \dot{p}_{cmd} \\ \dot{r}_{cmd} \end{bmatrix} = \begin{bmatrix} \cos(\alpha) & -\sin(\alpha) \\ \sin(\alpha) & \cos(\alpha) \end{bmatrix} \begin{bmatrix} v_{lat} \\ v_{dir} \end{bmatrix} \tag{1}$$

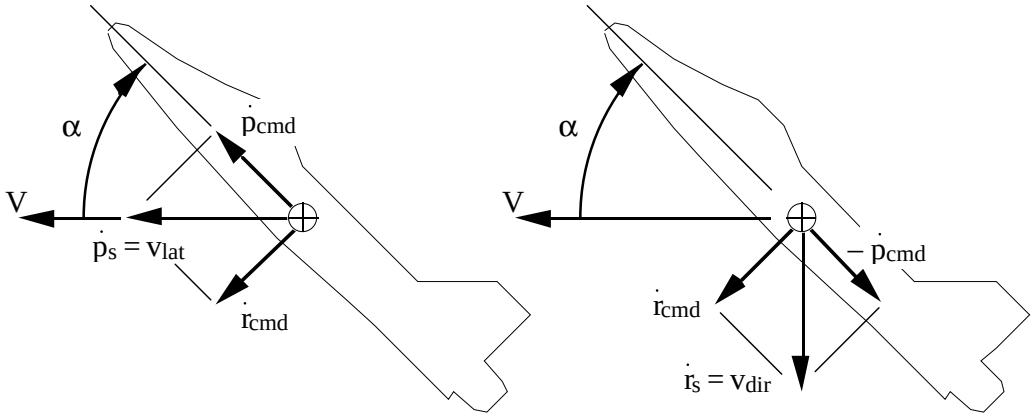

a) Lateral Command, v_{lat}. b) Directional Command, v_{dir}.

Figure 6. Stability-Axis Commands.

Moment Commands

The moments required to produce the desired roll and yaw accelerations are functions of the inertial characteristics of the airplane and the desired accelerations. Gyroscopic coupling also causes accelerations during airplane rotational motions. Additional moments required to cancel this inertial coupling are calculated as functions of the inertial characteristics and the angular body-axis rates of the airplane.

$$\begin{bmatrix} L_{cmd} \\ N_{cmd} \end{bmatrix} = \begin{bmatrix} I_{XX} & -I_{XZ} \\ -I_{XZ} & I_{ZZ} \end{bmatrix} \begin{bmatrix} \dot{p}_{cmd} \\ \dot{r}_{cmd} \end{bmatrix} + \begin{bmatrix} -I_{XZ} & I_{ZZ} - I_{YY} \\ I_{YY} - I_{XX} & +I_{XZ} \end{bmatrix} \begin{bmatrix} (p\,q) \\ (r\,q) \end{bmatrix} \tag{2}$$

The first term on the right-hand side of equation (2) translates the desired angular accelerations into the required body-axis moments and the second term compensates for inertial coupling.

Pseudo Control Variables

The above development yields the roll and yaw moments required for the airplane to respond to the stability-axis acceleration commands and to offset the effects of inertial coupling. The required moments

are divided by the available moments to yield *pseudo control variables* that indicate the fraction of the available moments needed. The roll pseudo control variable, v_{roll}, is the fraction of the available body-axis roll moment and the yaw pseudo control variable, v_{yaw}, is the fraction of the available body-axis yaw moment.

Roll control moments are generated by coordinated deflections of the conventional aerodynamic controls (ailerons, rudders, and differential motions of the horizontal stabilators) and may be supplemented with roll control moments generated by the thrust-vectoring system. Similarly, yaw control moments are generated by coordinated deflections of the conventional aerodynamic controls and may be supplemented with yaw control moments generated by the thrust-vectoring system and by differential deflections of the ANSER (actuated forebody strakes) controls.

Generation of yaw control moments by the thrust-vectoring system also causes rolling moments because the center of gravity of the airplane is displaced vertically from the line of thrust of the engines. This displacement is a vertical moment-arm on which the yaw-vectoring forces act, resulting in rolling moments. The ratio of the rolling moments to the yawing moments caused by yawing-moment commands equals the ratio of the vertical moment arm, l_z, to the distance that the thrust-vectoring apparatus is aft of the center of gravity, l_{TV}. The rolling moments are compensated by cross-feeding a portion of the yawing moment command into the rolling moment command.

$$v_{yaw} = N_{cmd} / N_{avail} \tag{3}$$

$$v_{roll} = \left[L_{cmd} - \frac{l_z}{l_{TV}} N_{TV}\, v_{yaw} \right] \Big/ L_{avail} \tag{4}$$

Roll Acceleration

The roll acceleration capability of the airplane about its stability axis is calculated. This value is provided for use in scheduling lateral (roll) commands derived from lateral motions of the control stick (see reference 11). Equations (5)–(7) are used to calculate this value. Figure 7 depicts the geometry upon which the equations are based.

$$\dot{p}_{s,max} = \dot{p}_{max} \cos\alpha + \dot{r}_{max} \sin\alpha \tag{5}$$

where

$$\dot{p}_{max} = \frac{L_{avail}}{I_{XX}} \tag{6}$$

$$\dot{r}_{max} = \frac{N_{avail}}{I_{ZZ}} \tag{7}$$

The calculated stability-axis roll acceleration capability is the sum of the contributions of the body-axis roll and yaw acceleration capabilities. The body-axis accelerations are calculated from the available roll and yaw moments and the body-axis moments of inertia. The effects of the cross product of inertia, I_{XZ}, are ignored. The calculations do not account for the balance between the roll and yaw axis controls required for coordination.

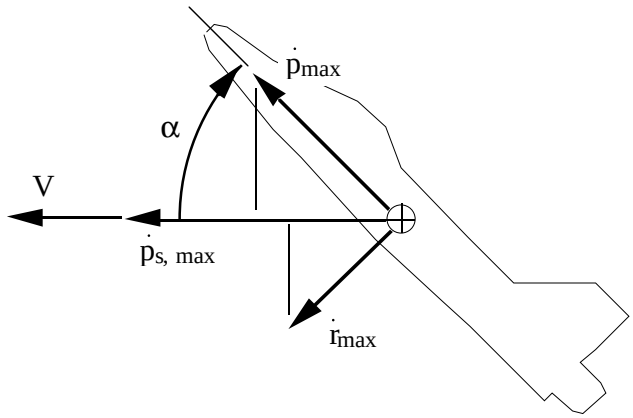

Figure 7. Maximum Stability-Axis Roll Acceleration.

Controls Distribution

This section describes the distribution of roll and yaw control commands to the conventional airplane lateral/directional flight controls (ailerons, rudders, and differential stabilators), the thrust-vectoring system, and to the actuated forebody strake controls. The controls are coordinated to provide a roll command channel and a yaw command channel. Commands to the roll command channel cause coordinated control deflections that produce body-axis roll moments with minimal yawing moments and commands to the yaw command channel produce body-axis yaw moments with minimal rolling moments. Side forces are not considered as an independent control influence in this development because they are closely related to the yaw control moments.

Distribution of Conventional Controls

The three conventional controls used for lateral and directional control are: (1) ailerons that are deflected differentially, (2) twin rudders that are deflected collectively, and (3) stabilators that are deflected differentially. These controls produce varying amounts of rolling moment, yawing moment, and side force depending on flight condition, especially dynamic pressure, angle of attack, and symmetric stabilator position. The object of the following development is to determine schedules for coordinating the conventional controls so that (1) rolling commands cause body-axis rolling moments with a minimum of yawing moment and (2) yawing commands cause body-axis yawing moments with minimum rolling moments. Additional schedules are determined that predict the rolling and yawing moments that can be generated by the conventional controls when operating according to the distribution schedules.

Control Moments – Conventional Controls

The roll and yaw moments generated by deflection of the conventional aerodynamic controls are given in equations (8) and (9).

$$L = \bar{q}\, S\, b \left(C_{l\delta a}\, \delta_a + C_{l\delta r}\, \delta_r + C_{l\delta d}\, \delta_d \right) \tag{8}$$

$$N = \bar{q}\, S\, b \left(C_{n\delta a}\, \delta_a + C_{n\delta r}\, \delta_r + C_{n\delta d}\, \delta_d \right) \tag{9}$$

The roll and yaw control coefficients are primarily functions of angle of attack and examples are given in figures 8 and 9. These figures depict the rolling and yawing moments produced by each of the conventional controls when deflected to its limit. These data were derived from a HARV simulation model (references 15 and 16) having the leading- and trailing-edge flaps in the clean configuration.

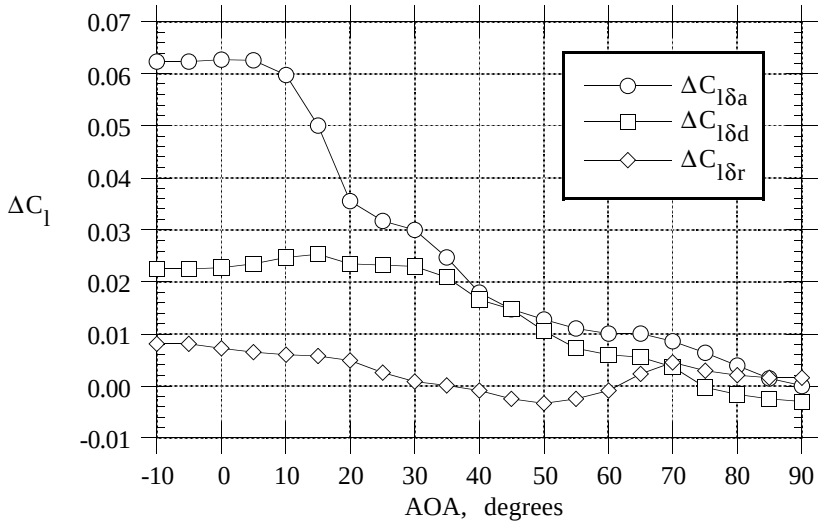

Figure 8. Example Roll Control Moment Coefficients of Conventional Controls, Mach 0.2, altitude 30 000 ft, stabilator –6.75 deg.

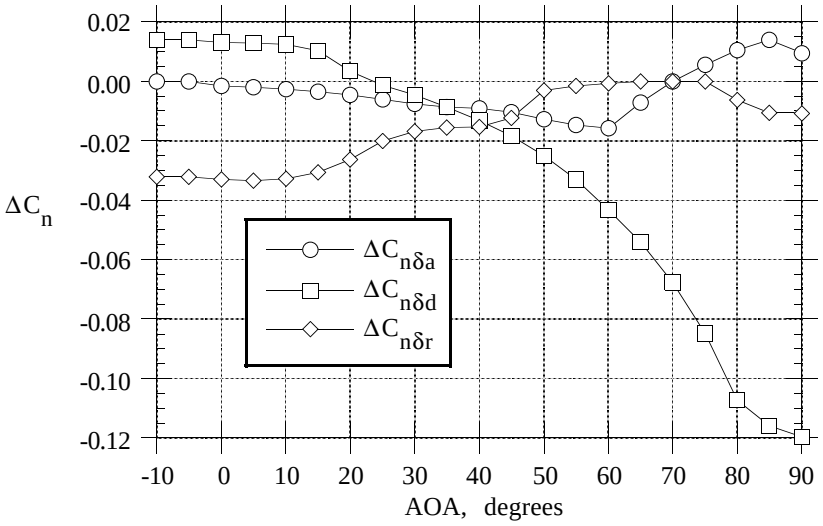

Figure 9. Example Yaw Control Moment Coefficients of Conventional Controls, Mach 0.2, altitude 30 000 ft, stabilator –6.75 deg.

Distribution Schedule Calculations

Let $\vec{u}$ be a vector containing the deflections of each of the conventional controls normalized by its maximum value. Let $\overrightarrow{c_{roll}}$ be a vector containing the roll moment coefficients that result from maximum deflection of each conventional control. Let $\overrightarrow{c_{yaw}}$ be a vector containing the yaw moment coefficients resulting from maximum deflection of each conventional control.

$$\vec{u} = \begin{bmatrix} \delta_a/\delta_{am} \\ \delta_r/\delta_{rm} \\ \delta_d/\delta_{dm} \end{bmatrix} \tag{10}$$

$$\overrightarrow{c_{roll}} = \begin{bmatrix} \Delta C_{l\delta a} \\ \Delta C_{l\delta r} \\ \Delta C_{l\delta d} \end{bmatrix} \tag{11}$$

$$\overrightarrow{c_{yaw}} = \begin{bmatrix} \Delta C_{n\delta a} \\ \Delta C_{n\delta r} \\ \Delta C_{n\delta d} \end{bmatrix} \tag{12}$$

The roll and yaw control coefficients for deflections of the conventional controls are calculated as the scalar products of equations (10) and (11), and of equations (10) and (12), respectively.

$$C_{roll} = \overrightarrow{c_{roll}}^{T} \vec{u} \tag{13}$$

$$C_{yaw} = \overrightarrow{c_{yaw}}^{T} \vec{u} \tag{14}$$

Let the normalized control deflections be specified by linear combinations of two control distribution vectors as follows.

$$\vec{u} = \overrightarrow{d_{roll}}\, v_{roll} + \overrightarrow{d_{yaw}}\, v_{yaw} \tag{15}$$

where v_{roll} and v_{yaw} are pseudo control variables for roll and yaw control moments, respectively, and where $\overrightarrow{d_{roll}}$ and $\overrightarrow{d_{yaw}}$ are the corresponding distribution vectors. Distribution vectors are desired such that the distribution vector for roll control, $\overrightarrow{d_{roll}}$, causes maximum rolling moment with a minimum yawing moment while the distribution vector for yaw control, $\overrightarrow{d_{yaw}}$, causes a maximum yawing moment with a minimum rolling moment. The roll distribution vector is the solution of the following optimization problem:

Find $\vec{d} = \overrightarrow{d_{roll}}$ to maximize

$$J = \vec{d}^{T} \overrightarrow{c_{roll}} \overrightarrow{c_{roll}}^{T} \vec{d} - \vec{d}^{T} \overrightarrow{c_{yaw}} \overrightarrow{c_{yaw}}^{T} \vec{d} \tag{16}$$

where

$$\vec{d}^{T} \vec{d} = (\text{constant})^2 \tag{17}$$

The roll distribution vector, $\overrightarrow{d_{roll}}$, is the eigenvector corresponding to the positive eigenvalue of the symmetric matrix W where

$$W = \overrightarrow{c_{roll}} \overrightarrow{c_{roll}}^{T} - \overrightarrow{c_{yaw}} \overrightarrow{c_{yaw}}^{T} \tag{18}$$

Conversely, the yaw distribution vector *minimizes* equation 16 subject to the constraint of equation 17. The yaw distribution vector, $\overrightarrow{d_{yaw}}$, is the eigenvector corresponding to the negative eigenvalue of matrix W. The third eigenvector of matrix W corresponds to a zero eigenvalue. This eigenvector lies in a control subspace that has no effect on the roll and yaw control moments and represents contradictory control deflections that cancel each other. Since the third eigenvector is not used by equation 15 in generating control deflections, contradictory control deflections are eliminated.

The pseudo control variables, v_{roll} and v_{yaw}, are dimensionless and range between –1.0 and +1.0 (see equation 15). The distribution vectors, $\overrightarrow{d_{roll}}$ and $\overrightarrow{d_{yaw}}$, are normalized to make their maximum elements unity. Distribution vector, $\overrightarrow{d_{roll}}$, contains the deflections of the conventional controls, normalized by their maximum values, that produce the maximum body-axis rolling moment within the capabilities of the controls. Likewise, distribution vector, $\overrightarrow{d_{yaw}}$, contains the normalized deflections of the controls that produce the maximum yawing moment.

Distribution Schedules

Several sets of data for the roll and yaw control coefficients as depicted in figures 8 and 9 were obtained. The data were taken for Mach numbers of 0.2, 0.4, 0.6, and 0.8; altitudes of 10 000 ft, 30 000 ft, and 50 000 ft; and symmetric tail deflections of –24.0 degrees (hard-over TEU), –15.375 degrees, –6.75 degrees (mid-range), +1.875 degrees, and +10.5 degrees (hard-over TED). The authority of the differential tail varies according to the symmetric tail position. The amount of free motion available for differential tail commands ranges from a maximum of ±17.25 degrees when the symmetric tail position is at the center of its range of travel to a minimum of zero when the symmetric tail position is hard-over in either direction.

Distribution schedules were calculated for each data set. The distribution schedules were averaged together and piecewise linear functions were fitted. The averaging was weighted to favor the trailing-edge-up data for large, post-stall angles of attack (≥ 44 degrees). The resultant distribution schedules for

roll and yaw control are presented in figures 10 and 11 with the normalization removed. The schedules for differential tail deflections are given for the symmetric tail at its mid-range value, –6.75 degrees, where the differential tail has the maximum authority of ±17.25 degrees. For other symmetric tail angles, the differential tail schedules must be reduced in proportion with the reduction in differential tail authority.

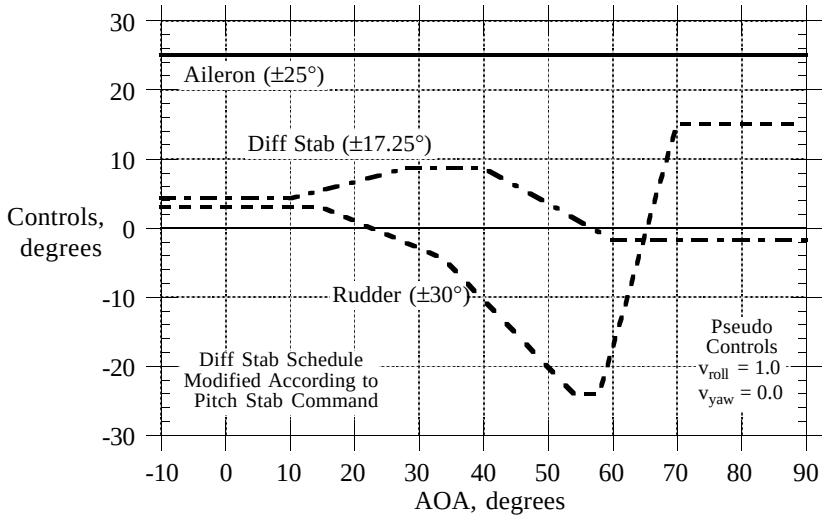

Figure 10. Roll Control Distribution Schedules.

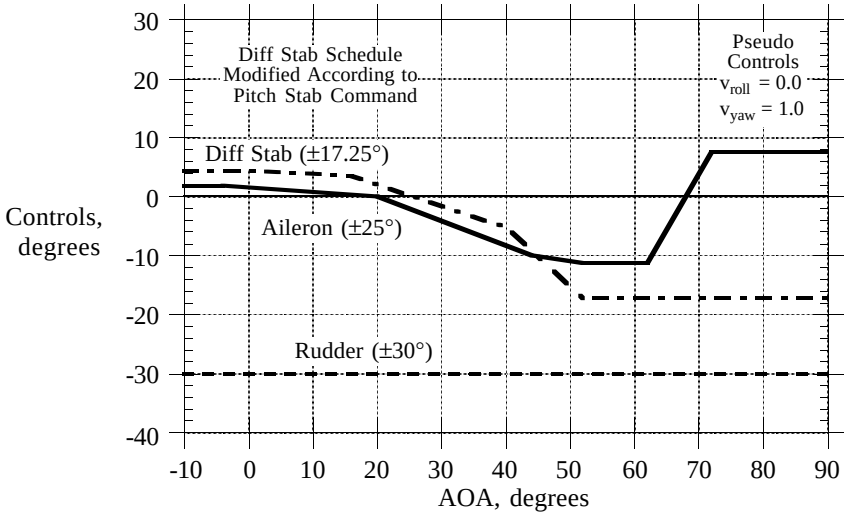

Figure 11. Yaw Control Distribution Schedules.

Conventional Controls Coefficients

In order to coordinate the lateral and directional axes of the airplane during flight through widely varying conditions with the possibility of engaging thrust-vectoring controls and actuated forebody strakes, it is necessary to calculate the roll and yaw control moments available from the different controls.

For the conventional controls, it is assumed that the above distribution schedules are effective in decoupling the roll and yaw axes. That is, the roll pseudo control variable, v_{roll}, causes body-axis roll moments while any yaw moments can be neglected. Similarly, the yaw pseudo control variable, v_{yaw}, causes body-axis yaw moments with negligible roll moments.

The roll coefficient produced by a unit of the roll pseudo control variable, v_{roll}, is calculated by combining equations (13) and (15) with the yaw pseudo control variable, v_{yaw}, set to zero (equation 19). Similarly, the yaw coefficient produced by a unit of the yaw pseudo controls variable is calculated by combining equations (14) and (15) with the roll pseudo control variable set to zero (equation 20).

$$\left.\frac{C_{roll}}{v_{roll}}\right|_{v_{yaw}=0} = \overrightarrow{c_{roll}}^{T}\,\overrightarrow{d_{roll}} \tag{19}$$

$$\left.\frac{C_{yaw}}{v_{yaw}}\right|_{v_{roll}=0} = \overrightarrow{c_{yaw}}^{T}\,\overrightarrow{d_{yaw}} \tag{20}$$

These coefficients were calculated using the above distribution schedules for $\overrightarrow{d_{roll}}$ and $\overrightarrow{d_{yaw}}$. The results were fitted with piecewise linear functions of angle of attack, differential tail authority, altitude, and Mach number. The roll and yaw controls coefficients corresponding to unity values of the roll and yaw pseudo control variables are plotted in figures 12 and 13, respectively, for 30 000 ft altitude and 0.2 Mach number.

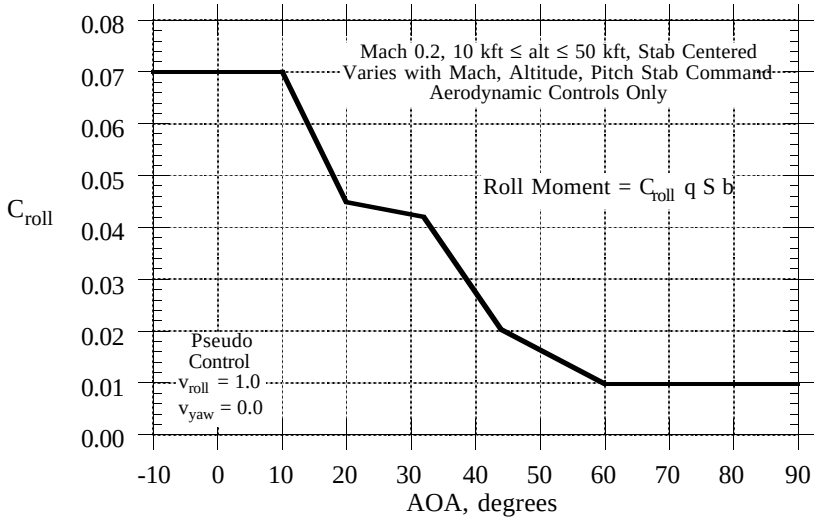

Figure 12. Total Available Roll Control Coefficient for Conventional Controls.

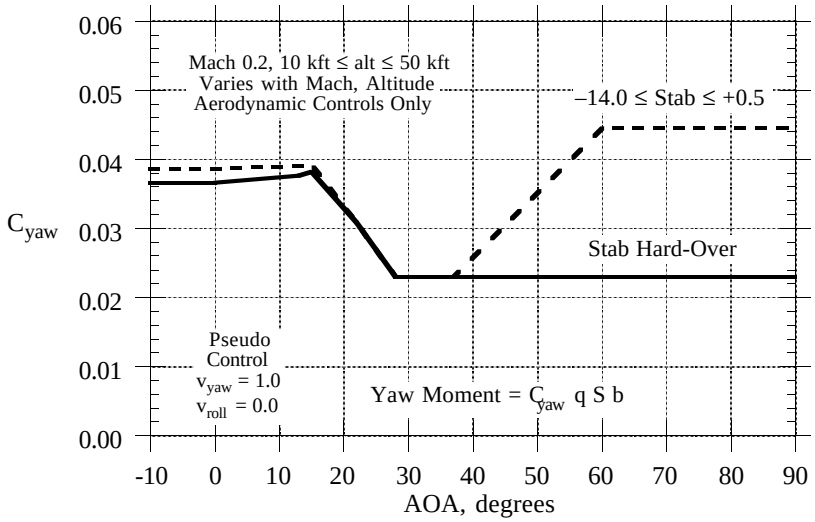

Figure 13. Total Available Yaw Control Coefficient for Conventional Controls.

The amount of rolling and yawing control moments that can be generated by the conventional controls are calculated by combining the coefficients with dynamic pressure.

$$L_{aero} = \bar{q}\, S\, b\, C_{roll} \tag{21}$$

$$N_{aero} = \bar{q}\, S\, b\, C_{yaw} \tag{22}$$

Distribution of Thrust-Vectoring Controls

The thrust-vectoring apparatus is designed to generate pitch, roll, and yaw control moments by deflecting the exhaust of the engines vertically and horizontally. Symmetric vertical deflections cause pitching moments, differential vertical deflections cause rolling moments, and horizontal deflections cause yawing moments. The roll and yaw thrust-vector angles are commanded in proportion to the roll and yaw pseudo control variables, respectively.

$$\delta_{TVr} = +\delta_{TVrm}\, v_{roll} \tag{23}$$

$$\delta_{TVy} = -\delta_{TVym}\, v_{yaw} \tag{24}$$

The thrust-vectoring control moments are proportional to the deflection angles and the thrust of the engines. The following equations describe the body-axis roll and yaw moments produced by the roll and yaw thrust-vectoring controls.

$$L = L_{TV}\, v_{roll} - \frac{l_z}{l_{TV}} N_{TV}\, v_{yaw} \tag{25}$$

$$N = N_{TV}\, v_{yaw} \tag{26}$$

The rolling moment capability of the rolling thrust-vector controls is a function of the maximum rolling thrust-vector angle, total engine thrust, and the lateral position of the engines.

$$L_{TV} = l_y \, T \left(\frac{\pi}{180} \right) \delta_{TVrm} \tag{27}$$

The yawing moment capability of the yawing thrust-vector controls is a function of the maximum yawing thrust-vector angle, total engine thrust, and the longitudinal distance between the thrust-vectoring nozzles and the airplane center of gravity.

$$N_{TV} = l_{TV} \, T \left(\frac{\pi}{180} \right) \delta_{TVym} \tag{28}$$

Distribution of Actuated Forebody Strake Controls

The actuated forebody strakes are mounted in a specially built radome. Each strake is actuated independently from a closed position (0 degrees) to a fully deployed position (90 degrees). These devices control the flow separation and vortices about the forward part of the airplane that induce moments that can be used for flight control. Wind tunnel studies have shown that actuated forebody strakes generate usable yawing control moments at elevated angles of attack (references 9 and 10). Rolling moments, however, are generally small. Therefore, for the design of the ANSER control system, the actuated forebody strakes are considered to be purely producers of yawing control moments.

Actuated Forebody Strake Dead-Band

During development of the ANSER control concept (reference 9), it was found that at higher angles of attack, deflecting one strake at a time could result in an undesirable control deadband or reversal for small strake deflections. When using the strake deflection schedule shown in figure 14a, positive differential strake commands, intended to generate negative (nose to the left) moments, produced deflections of the right strake with the left strake remaining at zero deflection (flush with the forebody). Similarly, negative differential commands caused deflections of only the left strake. However, it was found that the strakes must be commanded to a significant angle before yawing moments are produced in the desired direction,

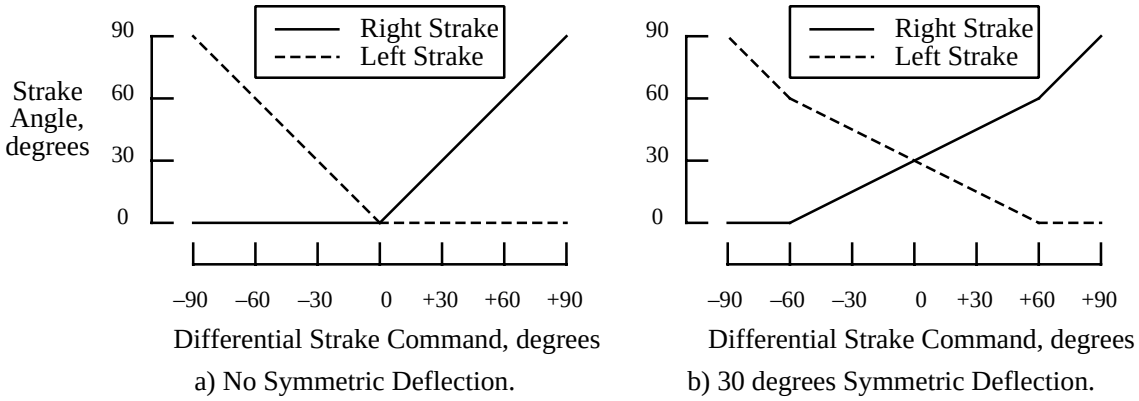

Figure 14. Actuated Forebody Strake Deflections versus Differential Strake Command.

especially at higher angles of attack. This leads to an objectionable deadband about the neutral command condition. A typical relationship between differential strake deflection and yawing moment is depicted as the solid line in figure 15. The deadband characteristic occurs above 30 degrees angle of attack and is most pronounced above 60 degrees.

The deadband characteristic was eliminated by incorporating a symmetric deployment schedule to the actuated forebody strake position commands. The schedule is a function of angle of attack and causes the strakes to deploy symmetrically when the angle of attack is large and the differential command is small. An example of the strake deflections versus differential command incorporating a symmetric deployment is shown in figure 14b. At zero differential command, both strakes are deflected to the required symmetric deployment angle. Differential control commands cause one strake to deflect further and the other to retract in unison until it becomes flush with the forebody. For larger differential commands, the strakes revert to the original schedule of figure 14a. The largest magnitude command (±90 degrees) results in one strake being fully deployed and the other being fully retracted. The symmetric deployment schedule 'linearizes' the control moment for small differential commands as depicted by the dashed line on figure 15.

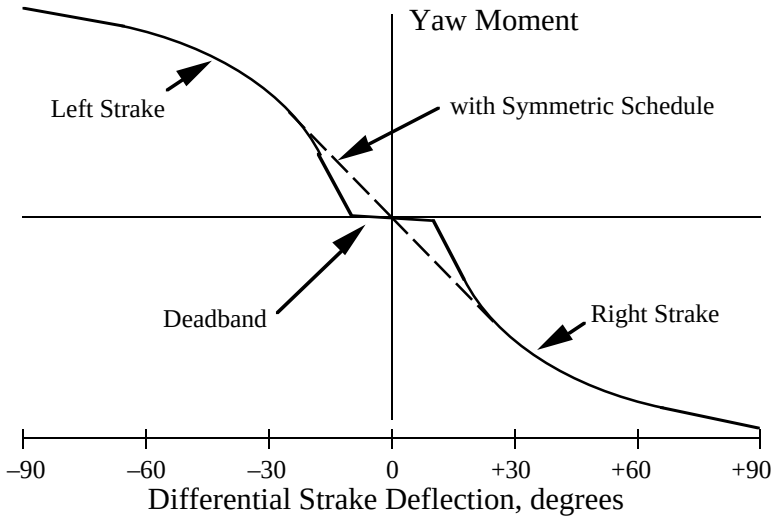

Figure 15. Actuated Forebody Strake Control Moments with and without Symmetric Strake Schedule.

Actuated Forebody Strake Calibration

Another nonlinearity of the yawing moment generated by the actuated forebody strakes is a variation of the incremental effectiveness depending on the amount of differential strake deflection. This is seen on figure 16 as a large reduction in the slope (by a factor of 2.75) at large differential deflection angles (solid line). This nonlinearity is corrected by driving the differential strakes by a nonlinear function of the yaw pseudo controls, v_{yaw}.

$$\delta_{FS} = -48 \left(1 + 0.875\, v_{yaw}^2\right) v_{yaw} \tag{29}$$

The term in the parentheses acts as a variable gain that reduces the slope of the yaw moment curve for small commands. The effect of the correction is shown by the dashed line in figure 16.

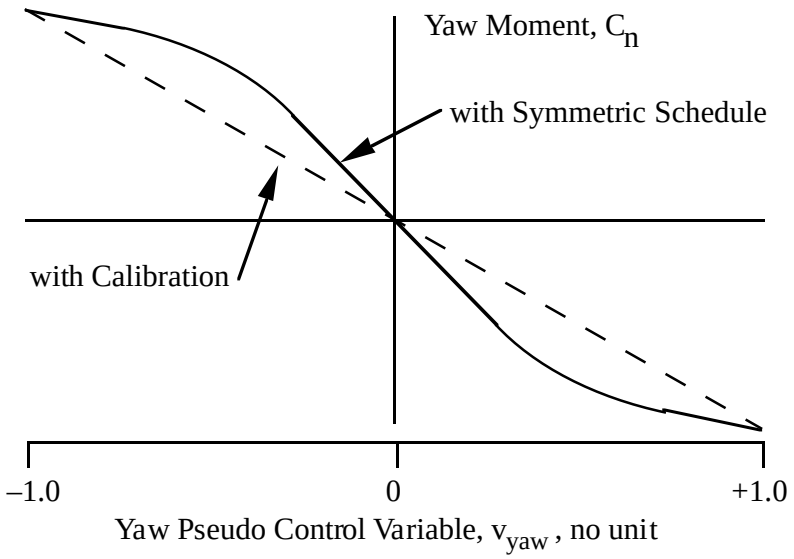

Figure 16. Actuated Forebody Strake Control Moment with and without Calibration.

The yawing control moment produced by full differential deflection of the actuated forebody strakes is a function of angle of attack depicted in figure 17. The yawing control moment that can be generated by the actuated forebody strakes is calculated by combining the control coefficient with dynamic pressure.

$$N_{FS} = \bar{q}\, S\, b\, \Delta C_{n,FS} \tag{30}$$

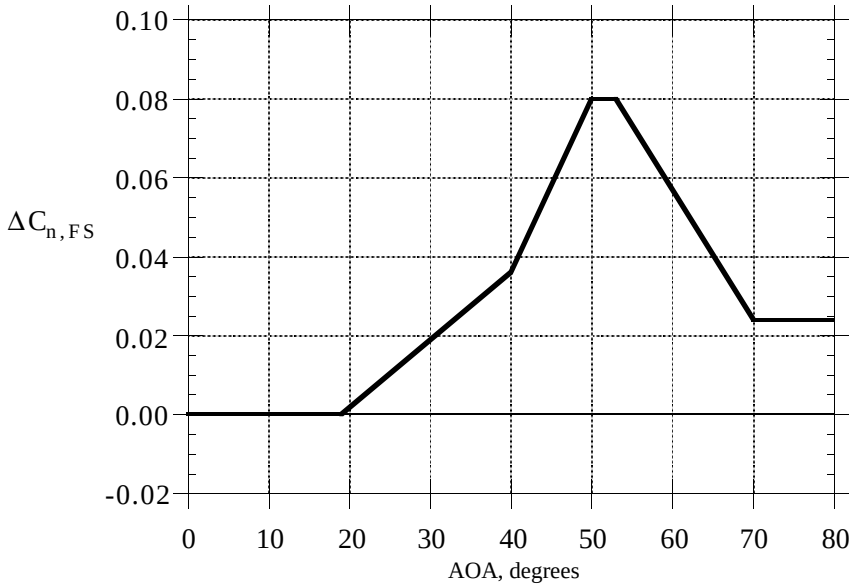

Figure 17. Available Actuated Forebody Strake Yaw Control Moment.

Controls Coordination

The controls distribution section has discussed the distribution of the roll and yaw pseudo controls variables, v_{roll} and v_{yaw}, to the conventional aerodynamic controls, equation (15), to the thrust-vectoring controls, equations (23) and (24), and to the actuated forebody strakes, equation (29). The range of each pseudo control variable is ±1.0 and it commands a specified fraction of the amount control moment for its axis of control. If v_{yaw} equals 0.2, for example, the conventional controls deflect to produce 20 percent of their yaw moment capability, the yaw thrust-vectoring apparatus deflects 20 percent, and the actuated forebody strakes deflect 20 percent. Operating in this manner, the different controls reach their limits as the pseudo control variable reaches unity magnitude.

Combining the roll and yaw moments produced by the conventional aerodynamic controls (equations 21 and 22), the thrust-vectoring controls (equations 25 and 26), and the actuated forebody strakes (equation 30), yields the body-axis roll and yaw moments as functions of the roll and yaw pseudo control variables.

$$L = \left[\bar{q}\ S\ b\ C_{roll} + L_{TV}\right] v_{roll} - \frac{l_z}{l_{TV}} N_{TV}\ v_{yaw} \tag{31}$$

$$N = \left[\bar{q}\ S\ b\ C_{yaw} + N_{TV} + \bar{q}\ S\ b\ \Delta C_{n,FS}\right] v_{yaw} \tag{32}$$

The controls distribution method discussed above converts the task of calculating command deflections of several control effectors (six in this case: ailerons, rudders, differential horizontal stabilizer, roll and yaw thrust vectoring controls, and differential forebody strakes) into one of specifying two pseudo control variables, one each for the roll and yaw airplane axes.

Accelerometer Correction

The lateral accelerometer in the original airplane design was located to minimize interference by the forces produced by the rudder. Rudder forces cause a linear acceleration and a rotational acceleration that combine to cause the airplane to initially rotate about a point forward of the center of gravity. Placement of the accelerometer at this point eliminates a direct coupling of the rudder forces to the accelerometer output that can interfere with control system operation. However, since the experimental thrust-vectoring system and the actuated forebody strakes are at different locations on the airplane, forces produced by them cause rotations about points that may be some distance from the accelerometer. Estimates of the interference terms are calculated in the control law and they are used to correct the accelerometer signal.

Figure 18 depicts a notional plan view of the airplane showing the placement of the thrust-vectoring system, the actuated forebody strakes, and the lateral accelerometer. The thrust-vectoring system generates forces, F_{TV}, concentrated at a distance, l_{TV}, aft of the c.g. The actuated forebody strakes generate forces, F_{FS}, concentrated at a distance, l_{FS}, forward of the c.g. Aerodynamic forces, F_{aero}, and moments, N_{aero}, that result in the usual accelerations at the sensor, are considered to act at the center of gravity. The lateral accelerometer is located at a distance, l_a, forward of the c.g.

The lateral acceleration of the center of gravity and the rotational acceleration are given by the following approximations:

$$a_{cg} = \frac{F_{aero} + F_{TV} + F_{FS}}{m} \tag{33}$$

$$\dot{r} = \frac{N_{aero} - l_{TV}F_{TV} + l_{FS}F_{FS}}{I_{ZZ}} \tag{34}$$

These equations are combined to yield the lateral acceleration at the sensor location.

$$a_y = \left[\frac{F_{aero}}{m} + l_a \frac{N_{aero}}{I_{ZZ}}\right] + \left[\frac{l_a}{I_{ZZ}} - \frac{l}{l_{TV}\, m}\right] N_{TV} + \left[\frac{l_a}{I_{ZZ}} + \frac{l}{l_{FS}\, m}\right] N_{FS} \tag{35}$$

where

$$N_{TV} = -l_{TV}F_{TV} \tag{36}$$

$$N_{FS} = l_{FS}F_{FS} \tag{37}$$

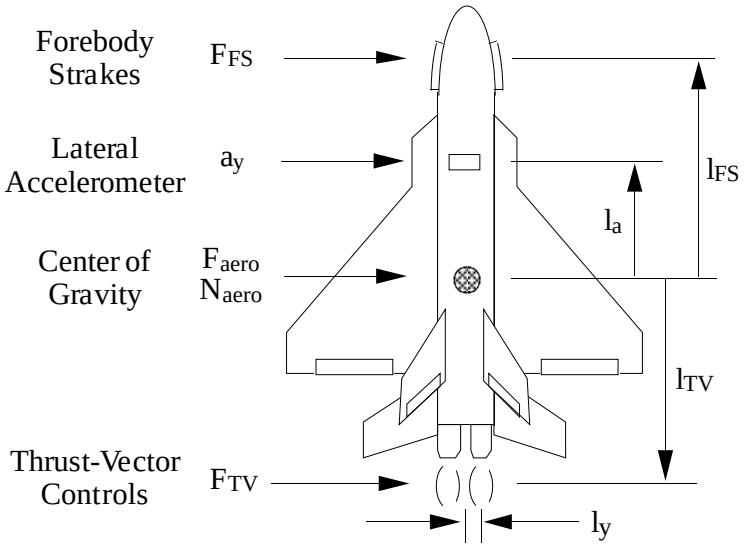

Figure 18. Plan view of Airplane Showing Lateral Accelerometer Interference.

The first term of equation (35) is the usual lateral acceleration at the sensor location and includes the effects of rudder control forces. The next two terms are interference caused by thrust-vectoring and actuated forebody strake forces, respectively. These terms may cause instantaneous response in the sensor signal to control commands that result in objectionable oscillations. They can also cause constant offsets of the sensor signal during steady maneuvers that can affect airplane performance. A correction for the accelerometer may be calculated using the interference terms of equation (35).

$$a_{y,corr} = \left[a_{y,corr}\, N_{TV} + a_{y,corr}\, N_{FS}\right] v_{yaw} \tag{38}$$

where

$$a_{y,TV} = \left[\frac{l_a}{I_{ZZ}} - \frac{l}{l_{TV}\, m} \right] \tag{38a}$$

$$a_{y,FS} = \left[\frac{l_a}{I_{ZZ}} - \frac{l}{l_{FS}\, m} \right] \tag{38b}$$

The calculation of the interference of thrust vectoring on the accelerometer (equation 38a) is obtained using airplane mass and dimensional data.

In order to calculate the interference of the actuated forebody strakes on the accelerometer (equation 38b), the ratio of the moment to force produced by differential strake deflections was calculated at each point in the database to obtain an effective moment arm, l_{FS}. An average value for the moment arm at each angle of attack was used. A schedule of the interference acceleration caused by actuated strake control moments as a function of angle of attack is presented in figure 19. The calculated data are shown as symbols and the schedule is shown as a line.

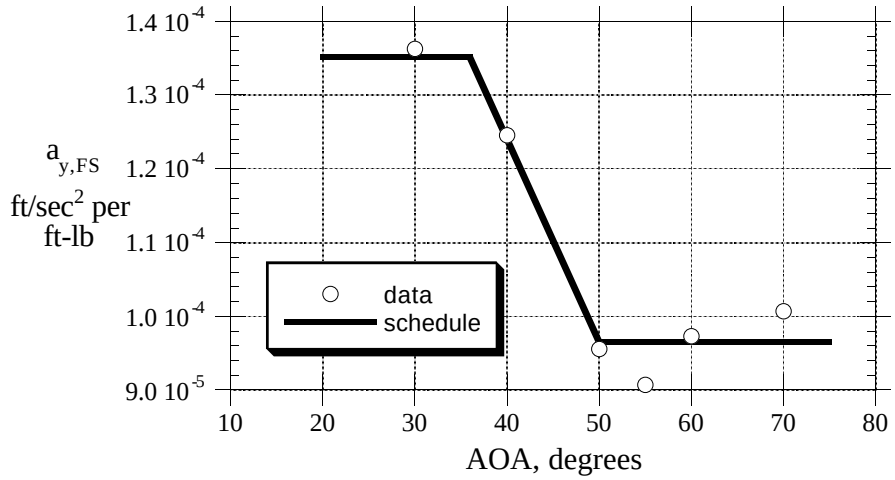

Figure 19. Lateral Accelerometer Correction for Actuated Forebody Strakes.

Thrust-Vectoring Engagement

This section describes the schedules that engage the yaw and roll thrust-vectoring controls as functions of flight condition and engine thrust level. The thrust-vectoring controls are regulated by scheduling variables S_{TVy} for the yaw axis and S_{TVr} for the roll axis. For each axis, the thrust-vectoring controls are engaged or 'on' when the scheduling variable is unity and are disengaged or 'off' when it is zero. Intermediate values of the scheduling variable cause partial engagement of the respecting thrust-vectoring control. The scheduling variables are used as multiplying gains on the thrust-vectoring commands. Equations (23) and (24) are rewritten to include the scheduling variables

$$\delta_{TVr} = \delta_{TVm}\, S_{TVr}\, v_{roll} \tag{39}$$

$$\delta_{TVy} = -\,\delta_{TVym}\, S_{TVy}\, v_{yaw} \tag{40}$$

The moment capabilities of the thrust-vectoring controls vary with the scheduling variables. Equations (27) and (28) are rewritten to include the scheduling variables

$$L_{TV} = l_y\, T \left(\frac{\pi}{180}\right) \delta_{TVrm}\, S_{TVr} \tag{41}$$

$$N_{TV} = l_{TV}\, T \left(\frac{\pi}{180}\right) \delta_{TVym}\, S_{TVy} \tag{42}$$

The accounting of the scheduled thrust-vectoring moments in the total available rolling and yawing control moments, L_{avail} and N_{avail}, used in equations (3) and (4) makes the rolling and yawing moments insensitive to the value of the schedule variables. For example, if thrust vectoring is turned on for either axis at some point in flight, the increased available control moment is accounted for by a reduction in the corresponding pseudo control variable. The subsequent reduction in the control moment produced by the aerodynamic controls is balanced by the control moment introduced by the thrust-vectoring control (assuming none of the controls is saturated). Within the accuracy of the design calculations, the airplane's flight behavior is unaffected when the thrust-vectoring controls are turned on or off. Therefore, the feedback gains used in a control system do not need to be adjusted and feedback loops do not need to be added to the control system to account for the presence of thrust-vectoring controls. However, command gains may be increased when thrust-vectoring controls are engaged to take advantage of the increased control power.

Thrust-Vectoring Schedules

The scheduling variables are determined using calculated values of the control moments available from the aerodynamic controls (including actuated forebody strakes, if used) and the control moments available from the thrust-vectoring controls. These moments are given by equations (21), (22), (27), and (28). The schedules cause the thrust-vectoring controls to be disengaged (scheduling variable = 0) when the aerodynamic controls are at least twice as powerful as the thrust-vectoring controls. Thrust-vectoring controls are fully engaged (schedule variable = 1) when they are at least as powerful as the aerodynamic controls.

$$S_{TVy} = \begin{cases} 0 & , \quad N_{TV} < \dfrac{1}{2} N_{aero} \\ 2 - \dfrac{N_{aero}}{N_{TV}} & , \quad \dfrac{1}{2} N_{aero} \le N_{TV} \le N_{aero} \\ 1 & , \quad N_{TV} > N_{aero} \end{cases} \tag{43}$$

$$S_{TVr} = \begin{cases} 0 & , \quad L_{TV} < \dfrac{1}{2} L_{aero} \\ 2 - \dfrac{L_{aero}}{L_{TV}} & , \quad \dfrac{1}{2} L_{aero} \le L_{TV} \le L_{aero} \\ 1 & , \quad L_{TV} > L_{aero} \end{cases} \tag{44}$$

Figure 20 depicts the yaw control moments produced by the aerodynamic controls and yaw thrust-vectoring controls as functions of dynamic pressure. Figure 20a depicts the aerodynamic and thrust-vectoring control moments individually. The aerodynamic control moment is proportional to dynamic pressure with a coefficient, C_{yaw}, of 0.04. This coefficient is representative of the yaw control capability of the HARV conventional controls at low angles of attack (see figures 9 and 13). The bold lines on figure 20a depict the yaw thrust-vectoring capability of the HARV for two thrust levels approximately equal to full- and half-thrust at test altitude. The yaw thrust-vectoring moments are calculated from equations 42 and 43. Figure 20b depicts the yaw control moment produced by the combination of the aerodynamic and thrust-vectoring controls. Line 0-① on the figure (from the origin to the point marked as ①) is the yaw moment produced by the aerodynamic controls only (also shown on figure 20a). Line 0-② is twice this yaw moment. The bold, solid line ③-④-⑤-① is the total yaw control moment when thrust is 15 000 lb. For higher airspeeds, dynamic pressure is large and yaw thrust vectoring is off.

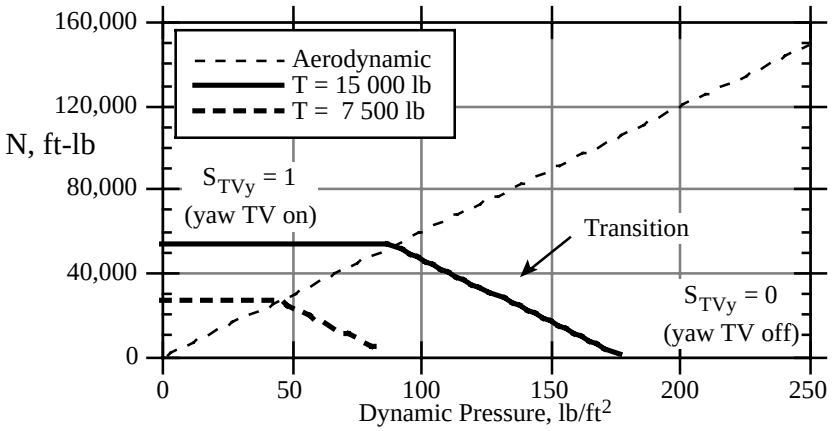

a) Individual Aerodynamic and Thrust-Vectoring Yaw Control Moments.

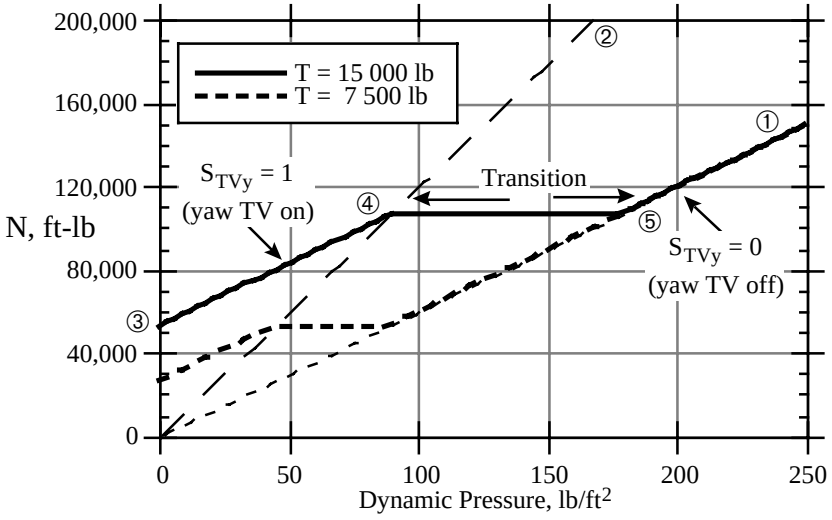

b) Combined Aerodynamic and Thrust-Vectoring Yaw Control Moments.

Figure 20. Yaw Thrust-Vector Schedules for $C_{yaw} = 0.04$.

Under these conditions, the yaw moment is given by the line segment ①-⑤. This corresponds to the first term of equation (43). In the transition region, the moment produced by the aerodynamic controls is between one and two times that available from the thrust-vectoring controls. The thrust-vectoring controls are scheduled on with decreasing dynamic pressure to maintain total control moment at a constant value equal to twice that available from the thrust-vectoring controls shown as line segment ④-⑤. This corresponds to the second term of equation (43). For low values of dynamic pressure, the thrust-vectoring controls are fully on and the yaw moment equals that of the aerodynamic controls plus that of the thrust-vectoring controls, depicted as line segment ③-④. This corresponds to the third term of equation (43). The effect of reducing thrust is depicted on figure 20b by the bold, dashed line. Since the yaw thrust-vectoring capability is reduced, the switch points, ④ and ⑤, are shifted to lower values of dynamic pressure.

Figure 21 depicts the roll control moment produced by the combination of the aerodynamic and thrust-vectoring controls. The aerodynamic control moment is proportional to dynamic pressure with a coefficient, C_{roll}, of 0.07. This coefficient is representative of the roll control capability of the HARV conventional controls at low angles of attack (see figures 8 and 12). Roll thrust-vectoring control can be used over a much smaller range of dynamic pressure than the yaw control because the close spacing of the engines results in a relatively weak roll moment producing capability.

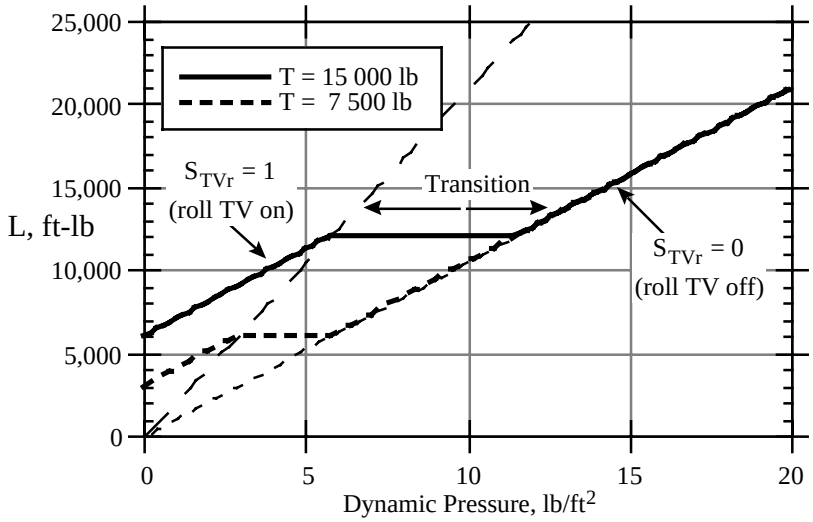

Figure 21. Roll Thrust-Vectoring Schedules for C_{roll} = 0.07.

Thrust-Vectoring Envelopes

Figures 22–24 illustrate the thrust-vectoring envelopes that result from using the schedules of equations (43) and (44). A number of points indicating level, nonaccelerating, 1g flight conditions are included on the figures for reference. Each figure shows boundaries between the thrust-vectoring-off region, the transition region, and the thrust-vectoring-on region. These are plotted against equivalent airspeed (KEAS) for a range of angle of attack. The boundaries are given for flight at 25 000 feet altitude using aerodynamic data for Mach 0.2 and a nominal thrust level of 15 000 pounds. On the boundaries between the thrust-vectoring-off and transition regions, the aerodynamic control moments are double the thrust-vectoring control moments. On the boundaries between the transition and the thrust-vectoring-on regions, the aerodynamic control moments equal the thrust-vectoring control moments. Changes in the boundary locations caused by varying aerodynamic control derivatives with altitude and Mach number

are relatively small and are not shown. Two sets of boundaries are plotted on each figure. The solid lines indicate boundaries for conditions where the stabilators are commanded hard-over to their travel limits by large longitudinal control commands preventing their use in producing rolling or yawing moments. The dashed lines indicate the boundaries when the stabilators are free to move ±10 degrees differentially. The yaw and roll moments available from differential stabilator deflections cause the boundaries to shift to slower airspeeds. The boundary locations are sensitive to changes in thrust caused by altitude changes, speed changes, and throttle position. Increases in thrust cause the boundaries to shift to higher airspeeds (upwards on the figures) and decreases in thrust cause shifts to lower airspeeds. The shifts follow a square root relationship with thrust such that a doubling of thrust causes the airspeeds to increase by a factor of the square root of two.

Figure 22 presents the yaw thrust-vectoring envelopes when the actuated forebody strakes are not used. For low angles of attack (less than 16 degrees), the yaw thrust-vectoring controls are off when airspeed is greater than 240 KEAS, and they are on when airspeed is less than 170 KEAS, with a transition between these airspeeds. For angles of attack between 16 and 28 degrees, the yaw control moment coefficient for the conventional controls decreases (see figure 13). Dynamic pressure must be increased in order to have the same control moments as at the lower angles of attack. Therefore, the boundaries shift to higher airspeeds for angles of attack between 16 and 28 degrees. The yaw control coefficient for the aileron-rudder combination is constant for angles of attack greater than 28 degrees. This results in the boundaries being at constant airspeeds for hard-over collective deflections of the stabilators (solid lines). When the stabilators are free to move differentially, they are effective in generating yaw moments at angles of attack greater than 38 degrees. This causes the boundaries to be at much lower airspeeds (dashed lines). For trimmed, 1g flight at small angles of attack, the airspeed is high and the aerodynamic yaw control moment is at least twice the thrust-vectoring control moment. Yaw thrust vectoring is off for these conditions. For large angles of attack, the airspeed is low and the aerodynamic moment is less than the thrust-vectoring moment. Yaw thrust vectoring is on for these conditions. Figure 22 does not give a precise indication of the on-off state of the thrust-vectoring controls for the trimmed flight conditions shown because the boundaries are calculated for a nominal thrust of 15 000 lb that is not necessarily the thrust for the trimmed conditions.

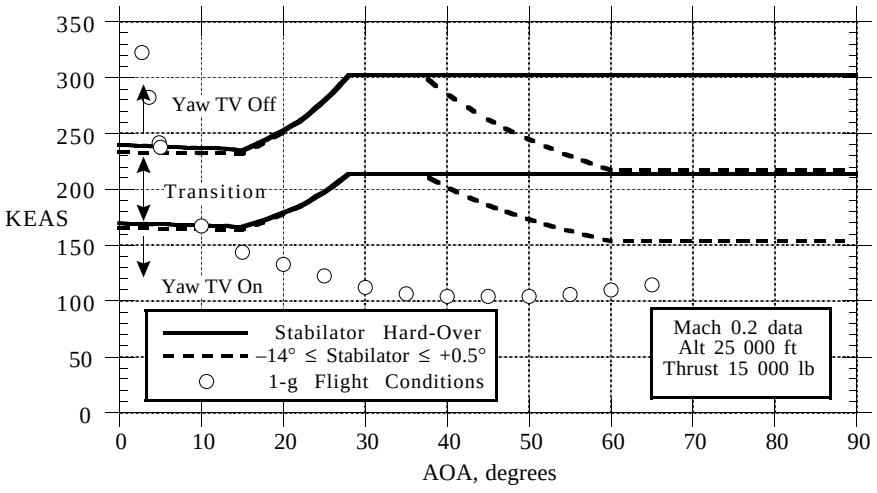

Figure 22. Yaw Thrust-Vectoring Envelopes without Actuated Forebody Strakes.

Figure 23 presents the yaw thrust-vectoring envelopes when the actuated forebody strakes are used. The figure is the same as figure 22 for angles of attack less than 19 degrees, because the forebody strakes produce no yaw control moments here. For angles greater than 19 degrees, the strakes produce yaw control moments, especially near 50 degrees of angle of attack. This causes the boundaries to be at much slower airspeeds than in figure 22 where strakes are not employed.

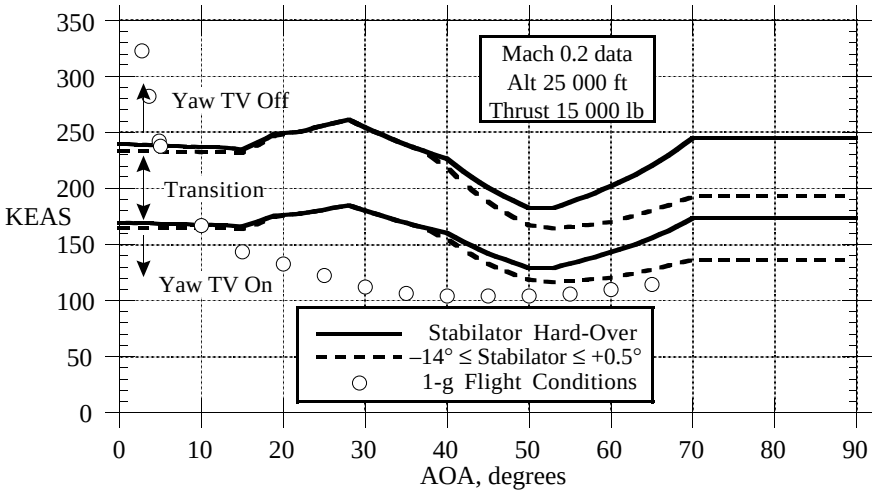

Figure 23. Yaw Thrust-Vectoring Envelopes with Actuated Forebody Strakes.

Figure 24 presents the roll thrust-vectoring envelopes. The figure shows roll thrust-vectoring controls being turned on between the very slow airspeeds of 40 and 60 KEAS at low angles of attack because they are very weak in comparison with the aerodynamic roll controls. The aerodynamic roll control coefficient is greatly diminished for large angles of attack (see figure 12). Therefore, the boundaries increase to 110 and 160 KEAS at 60 degrees angle of attack. Roll thrust-vectoring controls are scheduled off for 1g flight conditions at angles of attack less than 40 degrees and are scheduled on at 60 degrees. The boundaries are largely unaffected by the availability of differential stabilator controls (compare the solid lines with the dashed lines).

Although the control system includes roll thrust vectoring in the design, this feature was not used in the HARV flight test program because of interference from the priority limiting function of Mixer/Predictor program.

Vane Relief

Use of the thrust-vectoring vanes, unique for the HARV airplane, is restricted by heating constraints. In order to minimize vane heating, a ‘vane relief’ function was devised. This function transfers deflection commands from the thrust-vectoring controls to the aerodynamic controls to ‘wash-out’ the vane deflections while maintaining the commanded control moments. Other thrust-vectoring mechanisms that do not have such heating constraints would not require the use of the vane relief function. This section describes functions included in the control distribution portion of the system to reduce long-term deflections of the thrust-vectoring controls. The following discussion of the vane relief function can be applied to each of the control axes with an appropriate substitution of symbols and subscripts.

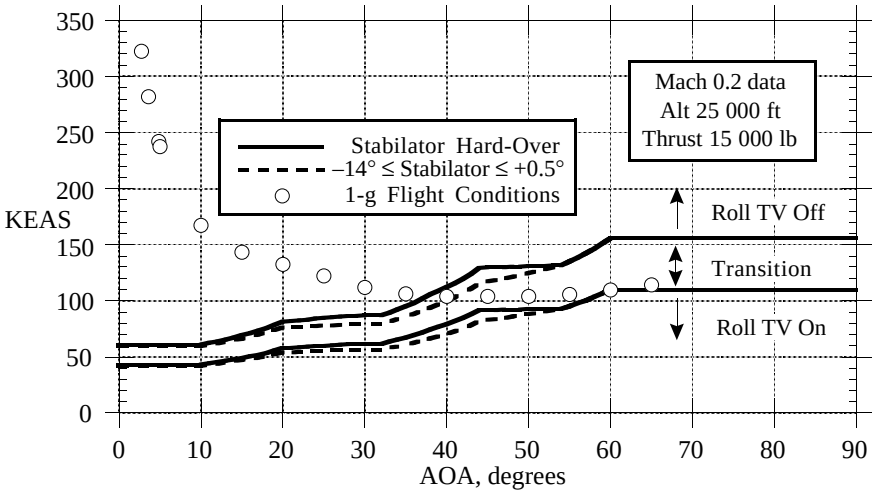

Figure 24. Roll Thrust-Vectoring Envelopes.

General Design

Figure 25 depicts the routing of control moment commands to the aerodynamic and thrust-vectoring controls used in the developments of the previous sections. This circuitry does not include vane relief.

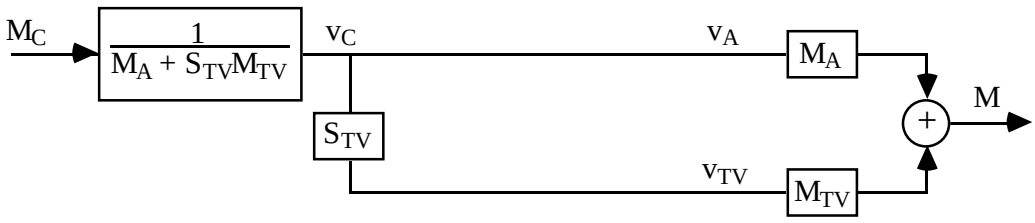

Figure 25. Block Diagram of Aerodynamic and Thrust-Vectoring Control Moments.

For each axis, the control moments generated by the aerodynamic controls and the thrust-vectoring apparatus sum together.

$$M = M_A\, v_A + M_{TV}\, v_{TV} \tag{45}$$

where

M	Total control moment, ft-lb
M_A	Available aerodynamic control moment, ft-lb
M_{TV}	Available thrust-vectoring control moment, ft-lb
v_A	Aerodynamic pseudo control variable (full throw at ±1)
v_{TV}	Thrust-vectoring pseudo control variable

The previous sections have stated that the aerodynamic and thrust-vectoring controls are deflected proportionally according to equations (46)–(48).

$$v_A = v_C \tag{46}$$

$$v_{TV} = S_{TV}\, v_C \tag{47}$$

$$v_C = \frac{M_C}{M_A + S_{TV} + M_{TV}} \tag{48}$$

where

M_C	Commanded control moment, ft-lb
S_{TV}	Thrust-vectoring engagement control (0 - off, 1 - on)
v_C	Command pseudo control variable

The command pseudo control variable, v_C, is the commanded control moment divided by the total available control moment.

Figure 26 depicts the routing of control moment commands to the aerodynamic and thrust-vectoring controls including the vane relief circuitry (enclosed within the shaded boundary).

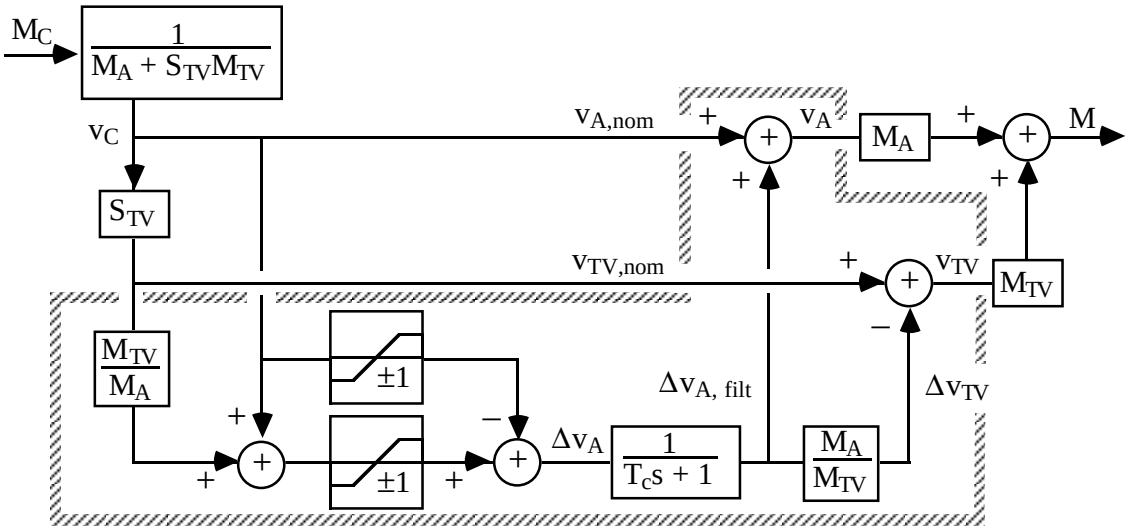

Figure 26. Block Diagram of Vane Relief Circuit.

The vane relief circuitry calculates a steady adjustment for the aerodynamic control that is the lessor of (1) the amount of aerodynamic control that would be required to generate the control moment that is produced by the thrust-vectoring control and (2) the amount of aerodynamic control that is available. The adjustment is modified by a low-pass filter and is added to the aerodynamic control variable. The amount of thrust-vectoring control required to compensate for the aerodynamic control modification is calculated

and this is subtracted from the thrust-vector control variable. The thrust-vector control is 'washed-out' to zero for steady commands so long as the aerodynamic control is strong enough to satisfy the command.

The commanded control moment, M_C, is divided by the total available control moment to produce the command pseudo control variable, v_C. The total available control moment is the sum of the available aerodynamic control moment, M_A, the product of the available thrust-vectoring control moment, M_{TV}, and the thrust vector engage variable, S_{TV}. The nominal aerodynamic pseudo control variable, $v_{A,nom}$ is set equal to v_C, and the nominal thrust-vectoring pseudo control variable, $v_{TV,nom}$ is set equal to v_C multiplied by the engage variable, S_{TV}. This part of figure 26 is the same as figure 25.

The nominal thrust-vectoring pseudo control variable, $v_{TV,nom}$ is multiplied by the ratio of the available thrust-vectoring control moment to the available aerodynamic control moment, M_{TV}/M_A, to calculate an equivalent amount of the aerodynamic pseudo control variable, v_A. This is added to the nominal aerodynamic pseudo control variable, $v_{A,nom}$, to calculate the aerodynamic control that would be required to produce the commanded moment if there were no thrust vectoring control. The sum is limited to ± 1 to keep it within the available range of the aerodynamic control. The nominal aerodynamic pseudo control variable, $v_{A,nom}$, is limited to unity and subtracted from this quantity to obtain the increment of the aerodynamic control, Δv_A, that can be commanded to alleviate the deflection of the thrust-vectoring control.

The increment, Δv_A, passes through a low-pass filter to limit vane relief to steady and slowly varying commands. The output of the filter, $\Delta v_{A,filt}$, is added to the aerodynamic pseudo control variable, v_A, to transfer the low-frequency part of the thrust-vectoring commands to the aerodynamic controls. This signal is also multiplied by the ratio of the aerodynamic control moment to the available thrust-vectoring control moment, M_A/M_{TV}, to calculate a change of the thrust-vectoring control, Δv_{TV}, that is equivalent to the change made to the aerodynamic control. This change is subtracted from the nominal thrust-vectoring pseudo control variable, $v_{TV,nom}$.

The moment, M, produced using the vane relief circuit is equal to the moment commanded, M_C (so long as limiting does not occur elsewhere), and is independent of the output of the filter and the increments being applied to the controls. When commanded moments are within the capability of the aerodynamic control alone, steady and slowly varying control actions are affected by the aerodynamic control while rapidly changing and high frequency control actions are affected by both the aerodynamic and thrust-vectoring controls. The characteristics of the filter used in the circuit determine the division between low frequency and high frequency operation. For the first-order filter shown in the figure, the 'crossover' frequency occurs at $1/T_c$ rad/sec. For a constant command, the thrust-vectoring control will seek its neutral condition so long as there is sufficient aerodynamic control power to satisfy the command at a rate depending on the value of the time constant. When steady commanded moments exceed the capability of the aerodynamic control alone, the aerodynamic control will seek its maximum value, $v_A = \pm 1$, while the thrust-vectoring control will deflect away from its neutral position to make up the deficit.

Figure 27 illustrates the operation of the vane relief logic for slowly varying and constant commands. The figure shows the moments generated by the aerodynamic and thrust-vectoring controls when the vane relief filter is at a steady-state condition. Figure 27a shows a case where the aerodynamic controls are more powerful than the thrust-vectoring control. In figure 27b, the thrust-vectoring control is stronger than the aerodynamic controls. The figures show the moments generated by the aerodynamic controls, $\leq M_A$, the thrust-vectoring control, $\leq M_{TV}$, and the total control moment, M, as functions of the commanded moment, M_C. Small commands, within the capability of the aerodynamic control alone, are

satisfied by the aerodynamic control with the thrust-vectoring control remaining at neutral. Larger commands result in maximum deflection of the aerodynamic controls with the thrust-vectoring controls used to make up the difference.

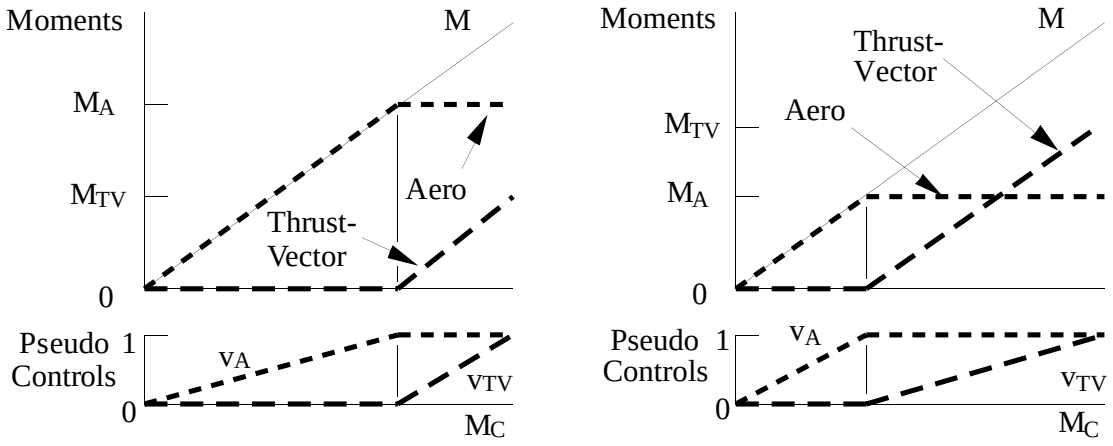

a) $M_A > M_{TV}$. b) $M_{TV} > M_A$.

Figure 27. Steady-State Vane-Relief Moments versus Command Moment.

Filter Time Constant

The vane relief function, as described above, is not acceptable for two reasons. First, for small moment commands, the vane relief function operates as a linear washout-type function. Linear operation implies that if the moment commands are small-amplitude sine waves, the outputs (surface deflections and thrust-vectoring commands) are sine waves also. Therefore, for sine wave commands, each thrust-vectoring vane is deflected into the engine exhaust jet 50 percent of the time. Since vane heating is a function of whether the vanes are deflected into the jet or not (rather than on the amount of the deflections into the jet), the vane relief function as described above fails to alleviate vane heating. Furthermore, if the moment command is a combination of a steady value with a rapidly varying sine wave superimposed upon it, the filter will move to a steady-state value according to the average value of the command and the average aerodynamic command and thrust-vectoring commands are adjusted as described above. The rapidly varying component is blocked by the filter and this component is passed to the aerodynamic and thrust-vectoring commands as in the previous figure. During periods of decreasing command magnitude, the aerodynamic and the thrust-vectoring controls may act in opposing directions. This is not acceptable because the aerodynamic and thrust-vectoring controls are in conflict. Both of these deficiencies are corrected by manipulating the time constant of the filter.

For increasing moment commands, the output of the filter, $\Delta v_{A,filt}$, lags the input, Δv_A. The increment subtracted from the thrust-vectoring command, Δv_{TV}, is less than the nominal thrust-vectoring command, $v_{TV,nom}$, resulting in incomplete cancellation. For such conditions the thrust-vectoring assists the aerodynamic controls so long as the command is increasing. The problem occurs when the command is being reduced. The lag of the filter causes the increment to be larger than the nominal thrust-vectoring command resulting in over-cancellation of the thrust-vectoring command. The aerodynamic commands become larger than they need to be to generate the commanded moment and the thrust-vectoring commands are in the opposite direction. In order to correct this operation, the filter is caused to quickly

bleed off as a function of its input and output values. The filter time constant varies according to figure 28.

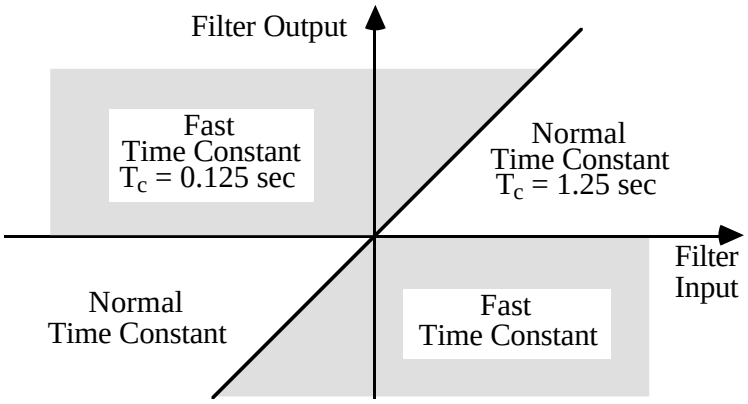

Figure 28. Variable Vane Relief Time Constant.

The filter operates with its normal time constant, T_c = 1.25 seconds, as long as the output is not greater than the input and the output has the same sign as the input . The region of normal operation is depicted as the wedge-shaped, clear areas on the figure. Should the operation of the filter leave this region, the filter time constant is decreased to 0.125 second. This causes the output to rapidly transition towards the normal operating region.

Simulation Example

Figure 29 presents time histories of the operation of the vane relief function. For this figure, the moment generating capabilities of the aerodynamic and thrust-vectoring controls are equal. The commanded moment (solid line on the top of the figure) is a sinusoidal function of varying frequency with an amplitude that is within the capability of either control. Without the vane relief function, the aerodynamic control (dashed line) and the thrust-vectoring control (dotted line) would be equal to half of the command. With the vane relief function, the filter output, shown at the bottom of the figure, is used to decrease the thrust-vectoring command with a compensating increase of the aerodynamic command to produce the data shown at the top of the figure. The time constant of the filter is shown in the center of the figure.

For the first 7 seconds of the time histories, the vane relief function causes most of the required moment to be generated by the aerodynamic control while reducing the thrust-vectoring contribution to a relatively small amount. The thrust-vectoring control is quickly reduced as the command decreases after 6 seconds. This is characteristic of a linear washout filter. At 7 seconds, the thrust-vectoring control reverses, becoming opposite in direction to the aerodynamic control. The time constant of the filter is reduced (to its fast value) to cause the filter to bleed rapidly so that the thrust-vector control remains near neutral and the commanded moment is mainly produced by the aerodynamic control. At 8.6 seconds the aerodynamic and thrust-vectoring controls are in the same direction, each equals one half of the command, and the filter output crosses zero. The filter time constant reverts to its normal high value (its slow value) and linear washout action resumes. As the frequency of the command increases, the vane relief function allows larger commands to the thrust-vectoring controls as the relief action diminishes.

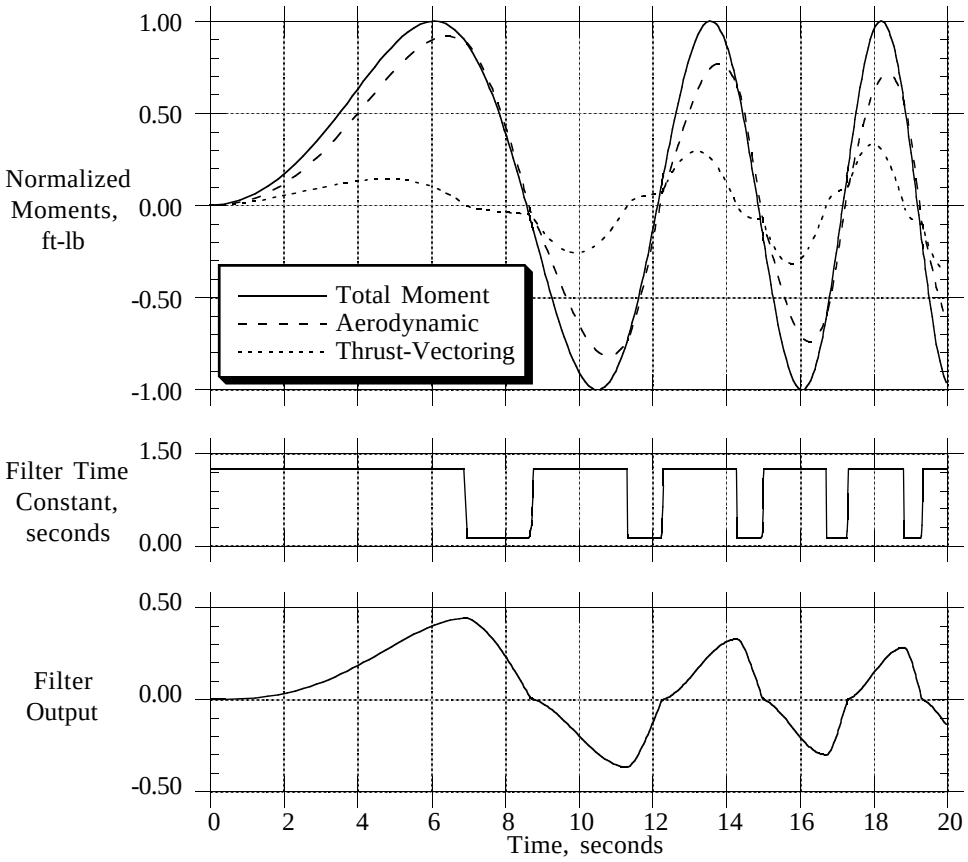

Figure 29. Simulated Vane Relief Operation.

Concluding Remarks

A method for integrating aerodynamic and thrust-vectoring controls for the control of flight to high angles of attack has been presented. Formulas were developed for the translation of roll and yaw acceleration commands into aerodynamic and thrust-vectoring control deflections. Sample data from the application of the method to the control of the High Angle-of-Attack Research Airplane (HARV) are included. The method has become known as the *pseudo controls* technique because of the use of normalized control variables (pseudo controls) that command coordinated aerodynamic and thrust-vectoring controls to produce uncoupled roll and yaw moments. The method does not include sensor feedback or pilot actions feed-forward elements of a control system that determine the required accelerations at any given time. The pseudo control system developed in the present report includes the following key elements:

- Transformation of stability-axis acceleration commands to body-axis acceleration commands.

- Calculation of body-axis control moments needed to produce the required accelerations and to counter inertial coupling effects.

- Calculation of the body-axis control moments available from coordinated control deflections and the fractions of these (pseudo controls) required to produce the required moments.

- Calculation of the maximum stability-axis roll acceleration possible with the available control moments (provided for use in pilot command gain).

- Distribution of roll and yaw pseudo controls to aerodynamic and thrust-vectoring control devices.

- Calculation of interference in the lateral accelerometer output caused by thrust-vectoring and actuated forebody strake control moments (for use in correcting acceleration feedback signals).

- Scheduling thrust-vectoring usage according to effectiveness relative to that of the aerodynamic controls.

- Replacing long-term thrust-vectoring commands by aerodynamic control deflections in order to relieve heating loads on exhaust jet turning vanes.

References

1. Matheny, Neil W., compiler: *High-Angle-of-Attack Projects and Technology Conference*. Volume 1, NASA CP-3137, 1992.

2. Barham, Robert W.: Thrust Vector Aided Maneuvering of the YF-22 Advanced Tactical Fighter Prototype. *AGARD Conference Proceedings 548: Technologies for Highly Maneuverable Aircraft*, March 1994.

3. Nguyen, Luat T.; Arbuckle, P. Douglas; and Gera, Joseph: Progress in Controls Technology for High-Angle-of-Attack Applications. *High-Angle-of-Attack Technology*, Volume I, CP-3149, NASA Langley Research Center, Hampton, VA, Oct. 30–Nov. 1, 1990, pp. 117–156.

4. Pahle, Joseph W.; Powers, Bruce; Regenie, Victoria; Chacon, Vince; Degroote, Steve; and Murnyak, Steven: *Research Flight-Control System Development for the F-18 High Alpha Research Vehicle*. NASA TM-104232, 1991.

5. Regenie, Victoria; Gatlin, Donald; Kempel, Robert; and Matheny, Neil: *The F-18 High Alpha Research Vehicle: A High-Angle-of-Attack Testbed Aircraft*. NASA TM-104253, 1992.

6. Mason, Mary L.; Capone, Francis J.; and Asbury, Scott C.: *A Static Investigation of the Thrust Vectoring System of the F/A-18 High-Alpha Research Vehicle*. NASA TM-4359, 1992.

7. Asbury, Scott C.; and Capone, Francis J.: *Multiaxis Thrust-Vectoring Characteristics of a Model Representative of the F-18 High-Alpha Research Vehicle at Angles of Attack From 0° to 70°.* NASA TP-3531, 1995.

8. Bundick, W. Thomas; Pahle, Joseph W.; Yeager, Jessie C.; and Beissner, Fred L., Jr.: *Design of a Mixer for the Thrust-Vectoring System on the High-Alpha Research Vehicle.* NASA TM-110228, 1996.

9. Murri, Daniel G.; Shah, Gautum H.; DiCarlo, Daniel J.; and Trilling, Todd W.: Actuated Forebody Strake Controls for the F-18 High-Alpha Research Vehicle. *J. Aircr*., vol. 32, no. 3, May–June 1995.

10. Erickson, Gary E.; and Murri, Daniel G.: *Wind Tunnel Investigations of Forebody Strakes for Yaw Control on F/A-18 Model at Subsonic and Transonic Speeds*. NASA TP-3360, 1993.

11. HARV Control Law Design Team: *Design Specification for a Thrust-Vectoring, Actuated-Nose-Strake Flight Control Law for the High-Alpha Research Vehicle*. NASA TM-110217, 1996.

12. Hoffler, Keith D.; Brown, Philip W.; Phillips, Michael R.; Rivers, Robert A.; Davidson, John B., Jr.; Lallman, Frederick J.; Murphy, Patrick C.; and Ostroff, Aaron J.: Evaluation Maneuver and Guideline Development for High-Alpha Control Law Design Using Piloted Simulation. AIAA 94-3512, Aug. 1994.

13. Ostroff, Aaron J.; Hoffler, Keith D.; and Proffitt, Melissa S.: *High-Alpha Research Vehicle (HARV) Longitudinal Controller: Design, Analyses, and Simulation Results*. NASA TP-3446, 1994.

14. Murphy, Patrick C.; and Davidson, John B.: *A Control Law Design Method Facilitating Control Power, Robustness, Agility, and Flying Qualities Tradeoffs: CRAFT*. NASA/TP-1998-208463, 1998.

15. Buttrill, Carey S.; Arbuckle, P. Douglas; and Hoffler, Keith D.: *Simulation Model of a Twin-Tail, High Performance Airplane*. NASA TM-107601, 1992.

16. Messina, Michael D.; Strickland, Mark E.; Hoffler, Keith D.; Carzoo, Susan W.; Bundick, W. Thomas; Yeager, Jessie W.; and Beissner, Fred L., Jr.: *Simulation Model of the F/A-18 High Angle of Attack Research Vehicle Utilized for the Design of Advanced Control Laws*. NASA TM-110216, 1996.

17. *Advanced Continuous Simulation Language (ACSL) Reference Manual*. Edition 10.0, Mitchell and Gauthier Assoc., 1991.

18. Ashworth, B. R.; and Kahlbaum, W. M., Jr.: *Description and Performance of the Langley Differential Maneuvering Simulator*. NASA TN D-7304, 1973.

19. Lallman, Frederick J.: *Relative Controls Effectiveness Technique with Application to Airplane Control Coordination*. NASA TP-2416, 1985.

20. Lallman, Frederick J.: *Preliminary Design Study of a Lateral-Directional Control System Using Thrust Vectoring*. NASA TM-86425, 1985.

REPORT DOCUMENTATION PAGE

Form Approved
OMB No. 07704-0188

1. AGENCY USE ONLY *(Leave blank)*	2. REPORT DATE	3. REPORT TYPE AND DATES COVERED
	September 1998	Technical Publication

4. TITLE AND SUBTITLE
A Method for Integrating Thrust-Vectoring and Actuated Forebody Strakes With Conventional Aerodynamic Controls on a High-Performance Fighter Airplane

5. FUNDING NUMBERS
WU 522-22-21-03

6. AUTHOR(S)
Frederick J. Lallman, John B. Davidson, and Patrick C. Murphy

7. PERFORMING ORGANIZATION NAME(S) AND ADDRESS(ES)
NASA Langley Research Center
Hampton, VA 23681-2199

8. PERFORMING ORGANIZATION REPORT NUMBER
L-17627

9. SPONSORING/MONITORING AGENCY NAME(S) AND ADDRESS(ES)
National Aeronautics and Space Administration
Washington, DC 20546-0001

10. SPONSORING/MONITORING AGENCY REPORT NUMBER
NASA/TP-1998-208464

11. SUPPLEMENTARY NOTES

12a. DISTRIBUTION/AVAILABILITY STATEMENT
Unclassified–Unlimited
Subject Category 08 Distribution: Standard
Availability: NASA CASI (301) 621-0390

12b. DISTRIBUTION CODE

13. ABSTRACT ***(Maximum 200 words)***

A method, called pseudo controls, of integrating several airplane controls to achieve cooperative operation is presented. The method eliminates conflicting control motions, minimizes the number of feedback control gains, and reduces the complication of feedback gain schedules. The method is applied to the lateral/directional controls of a modified high-performance airplane. The airplane has a conventional set of aerodynamic controls, an experimental set of thrust-vectoring controls, and an experimental set of actuated forebody strakes. The experimental controls give the airplane additional control power for enhanced stability and maneuvering capabilities while flying over an expanded envelope, especially at high angles of attack.

The flight controls are scheduled to generate independent body-axis control moments. These control moments are coordinated to produce stability-axis angular accelerations. Inertial coupling moments are compensated. Thrust-vectoring controls are engaged according to their effectiveness relative to that of the aerodynamic controls. Vane-relief logic removes steady and slowly varying commands from the thrust-vectoring controls to alleviate heating of the thrust turning devices. The actuated forebody strakes are engaged at high angles of attack.

This report presents the forward-loop elements of a flight control system that positions the flight controls according to the desired stability-axis accelerations. This report does not include the generation of the required angular acceleration commands by means of pilot controls or the feedback of sensed airplane motions.

14. SUBJECT TERMS
F/A-18 High-alpha research vehicle (HARV); Actuated nose strakes for enhanced rolling (ANSER); Fighter aircraft; Flight controls; Airplane control; Control design; Thrust vectoring; Forebody strakes; Forebody controls; High angle of attack; Integrated control

15. NUMBER OF PAGES
45

16. PRICE CODE
A03

17. SECURITY CLASSIFICATION OF REPORT	18. SECURITY CLASSIFICATION OF THIS PAGE	19. SECURITY CLASSIFICATION OF ABSTRACT	20. LIMITATION OF ABSTRACT
Unclassified	Unclassified	Unclassified	